Specific Propyne Trapping Sites within a Robust MOF for Efficient Propyne/Propadiene Separation with Record Propadiene Productivity

Yunjia Jiang, Lingyao Wang, Jianbo Hu, Rajamani Krishna, Banglin Chen,* and Yuanbin Zhang*

Separating propyne/propadiene to produce pure propadiene is extremely challenging in industry due to their similar properties. Herein, a novel ZrF_6^{2-} anion pillared cage-like metal-organic framework (termed as CuZrF$_6$-TPA) for highly efficient propyne/propadiene separation is reported. It exhibits high propyne capacity (177.4/188.6 cm^3/cm^3 at 0.5/1.0 bar and 298 K), benchmark separation selectivity (6.0), and remarkable separation potential (5.7 mol L^{-1}) simultaneously. Record propadiene productivity ($\approx$4.7 mol L^{-1}) is achieved through a single adsorption process in breakthrough experiments with excellent recycle stability even under humid conditions. Based on the structure of propyne-loaded single crystals, two binding sites are identified, including a major propyne trapping site at the windows and a minor binding site located in the large cages. Modelling studies further confirm that the contracted cage windows surrounded with rotating Lewis basic F atoms and aromatic rings are the optimal bonding sites to capture propyne with multiple hydrogen bonding and $\pi\cdots\pi$ interactions.

1. Introduction

Propadiene (CH$_2$ = C = CH$_2$) as the simplest allene is a significant building block in organic synthesis.[1] It is commonly used as a precursor for the preparation of versatile products via hydrofunctionalization, propargylation, cyclization, etc.[2,3] The utilization of propadiene in toluene is reported to serve as an atom economic motif that can be functionalized to realize the allylation of multiple pronucleophiles.[4] Currently, the production of pure propadiene relies on chemical synthesis, which suffers several disadvantages such as low productivity, inevitable waste by-products and high energy consumption, leading to the high cost of pure propadiene.[5,6] Therefore, it is imperative to develop new, effective and low-cost approaches to produce propadiene. Hydrocarbon cracking stands among the largest-scale chemical procedures globally, which produced 140 million tons of propylene in 2020. Propadiene and propyne are produced as by-products, constituting approximately 1–10% in the raw C$_3$ fraction.[7] On the other hand, the mixture of propyne, propadiene and propane, known as MAPP gas for welding and cutting applications,[8] is also a good source for propadiene. However, the separation of propadiene from propyne is extremely challenging due to the similar boiling points (difference = 10.8 °C) and closely matched molecular sizes (difference ≤ 0.2 Å) (Table S3, Supporting Information). To date, there is still no effective means for purifying propadiene,[9,10] culminating in the prevalent practice of processing propadiene-containing mixtures as industrial fuel-a course of action that begets significant waste.

Physical adsorption based on porous adsorbents has been a promising alternative method for gas separation with the advantages of low energy consumption and easy operation.[11–24] However, the use of traditional porous materials such as zeolites and activated carbon to separate propyne/propadiene has thus far yielded unsuccessful outcomes.[25] Nowadays, metal-organic-frameworks (MOFs) have been recognized as a prospective class of porous materials owing to their designable pore characteristics.[26–41] Large amounts of MOFs have been developed for the efficient separations of acetylene/ethylene (C$_2$H$_2$/C$_2$H$_4$),[42–46] propyne/propylene (C$_3$H$_4$/C$_3$H$_6$)[47–51] or propylene/propane (C$_3$H$_6$/C$_3$H$_8$)[52–56] with high selectivity. Nonetheless, the separation of propyne/propadiene (C$_3$H$_4$ isomers) is still an unsolved quandary because of the extremely

Y. Jiang, L. Wang, B. Chen, Y. Zhang
Key Laboratory of the Ministry of Education for
Advanced Catalysis Materials
College of Chemistry and Materials Science
Zhejiang Normal University
Jinhua 321004, China
E-mail: banglin.chen@fjnu.edu.cn; ybzhang@zjnu.edu.cn
J. Hu
Zhejiang Lab
Hangzhou 311100, P. R. China
R. Krishna
Van't Hoff Institute for Molecular Sciences
University of Amsterdam
Amsterdam 1098 XH, Netherlands
B. Chen
Fujian Provincial Key Laboratory of Polymer Materials
College of Chemistry & Materials Science
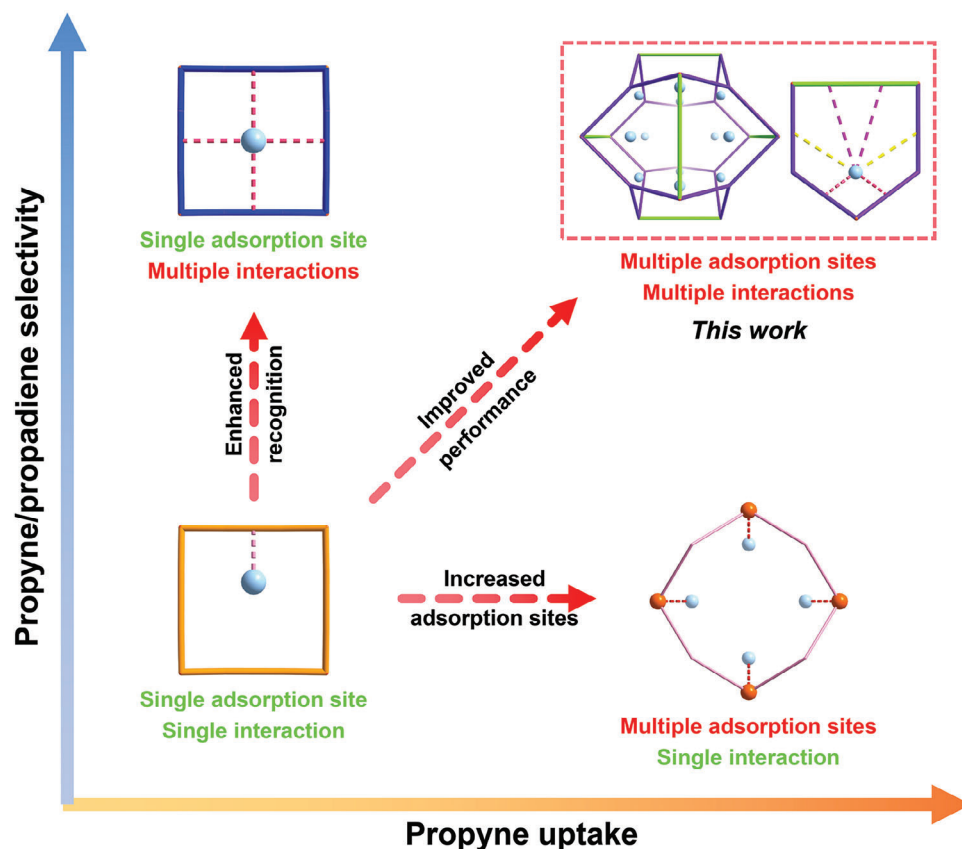Fujian Normal University
Fuzhou 350007, P. R. China

**ADVANCED
SCIENCE NEWS**

www.advancedsciencenews.com
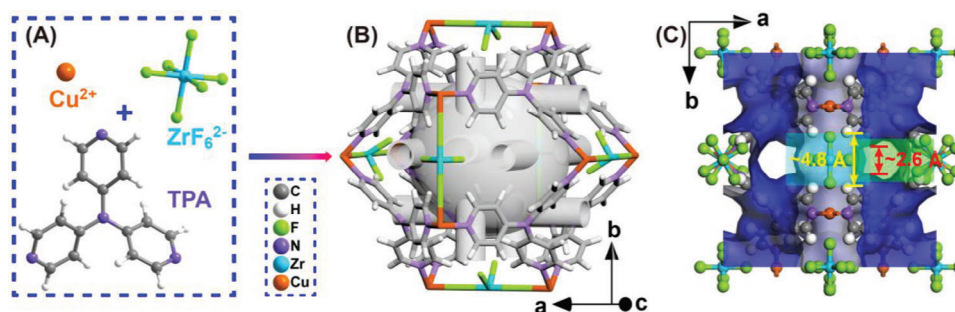
**ADVANCED
MATERIALS**

www.advmat.de

Scheme 1. The strategy of creating multiple adsorption sites and multiple supramolecular interactions in MOFs for boosting the propyne/propadiene separation performance.

similar molecular size and nearly indistinguishable polarizability (Table S3, Supporting Information). So far, less than 20 MOFs have been studied for the separation of propyne/propadiene and merely four MOFs, namely MOF-505 (Cu$_2$(bptc), bptc = 3,3′,5,5′-biphenyltetracarboxylate), Mg-MOF-74 (Mg$_2$(dobdc), dobdc = 2,5-dihydroxyterephthalate), NKMOF-1-Ni (Cu[Ni(pdt)$_2$], pdt = pyrazine-2,3-dithiol) and HKUST-1 (Cu$_3$(btc)$_2$, btc = benzene-1,3,5-tricarboxylate), have demonstrated the capability to achieve practical propyne/propadiene separation.[25] Among them, MOFs featuring multiple supramolecular interactions (e.g., NKMOF-1-Ni) with propyne can provide good separation selectivity of propyne/propadiene, yet the propyne uptake is low due to the limited adsorption sites; other MOFs (e.g., HKUST-1, Mg-MOF-74 and MOF-505) with multiple adsorption sites can afford a high uptake of propyne; however, the selectivity is sacrificed owning to the mediocre recognition ability of single open metal interaction. The high-performance porous materials for this very challenging need should have both high gas uptake and gas separation selectivity, and thus to overcome the above typically observed trade-off phenomenon. Therefore, it is highly demanding to develop novel advanced porous materials with multiple adsorption sites and multiple supramolecular interactions to achieve the challenging propyne/propadiene separation (**Scheme 1**).

Anion pillared MOFs (APMOFs) are a specific class of hybrid crystalline frameworks constructed by organic linkers, inorganic pillars and metal ions.[57–69] Due to the incorporation of inorganic anions, the pore surface is markedly polarized and can be used to discriminate the light hydrocarbons based on the hydrogen atom acidity. However, the investigations into APMOFs, including but not limited to SIFSIX-2-Cu-i (SIFSIX = SiF$_6$$^{2-}$; 2 = 4,4′-dipyridylacetylene; i = interpenetrated), SIFSIX-3-Ni (3 = pyrizine), UTSA-200 (SIFSIX-14-Cu-i, 14 = 4,4′-azopyridine), and ZU-62 (NbOFFIVE-2-Cu-i, NbOF-FIVE = NbOF$_5$$^{2-}$), have proven unsuccessful in the endeavor to yield high-purity propadiene.[25] We attribute this failure to the limited adsorption sites resulted from the over-constricted 1D channel pores in the investigated APMOFs. Instead, if we can construct APMOFs with multiple adsorption sites and abundant supramolecular interactions, commendable selectivity and high capacity may be achieved simultaneously.

With this in mind, we reported herein a novel ZrF$_6$$^{2-}$ anion hybrid MOF (termed as CuZrF$_6$-TPA, TPA = tri(pyridin-4-yl)amine) with capacious cage-like pores and specific anionic propyne trapping sites for benchmark propyne/propadiene separation. CuZrF$_6$-TPA exhibits excellent water and thermal stability. Adsorption measurements at 298 K on CuZrF$_6$-TPA indicated that the propyne uptake can reach up to 177.4 and 188.6 cm^3 cm^{-3} at 0.5 and 1.0 bar. The IAST selectivities of propyne/propadiene (50/50, 25/75) are both the record high of 6.0. The calculated Q$_{st}$ values for propyne and propadiene are 46.1 and 37.1 kJ mol^{-1}, allowing for ready regeneration of the

**ADVANCED
SCIENCE NEWS**

www.advancedsciencenews.com

**ADVANCED
MATERIALS**

www.advmat.de

Figure 1. A) Basic units to construct CuZrF$_6$-TPA; B) The structure of large pore with twelve windows; C) The voids of CuZrF$_6$-TPA illustrating the size of window sites, voids generated with a probe of 1.2 Å radius.

material under mild conditions. Besides, the separation potentials of CuZrF$_6$-TPA for 50/50 and 25/75 propyne/propadiene mixtures were calculated as high as 5.7 and 12.8 mol L^{-1}, respectively. Propyne-loaded single crystal structure and DFT calculations both indicated that the cage window sites with multiple rotating anionic F atoms and aromatic rings are the optimal bonding sites to capture propyne via synergistic C-H···F/C-H···C hydrogen bonding and π···π interactions. Dynamic breakthrough experiments were conducted to evaluate the practical separation performance. In each adsorption process, significantly high propadiene productivity ($\approx$4.7 mol L^{-1}) was obtained from equimolar propyne/propadiene mixture. The separation performance was retained under humidity, under different flowing rates and over twelve recycles.
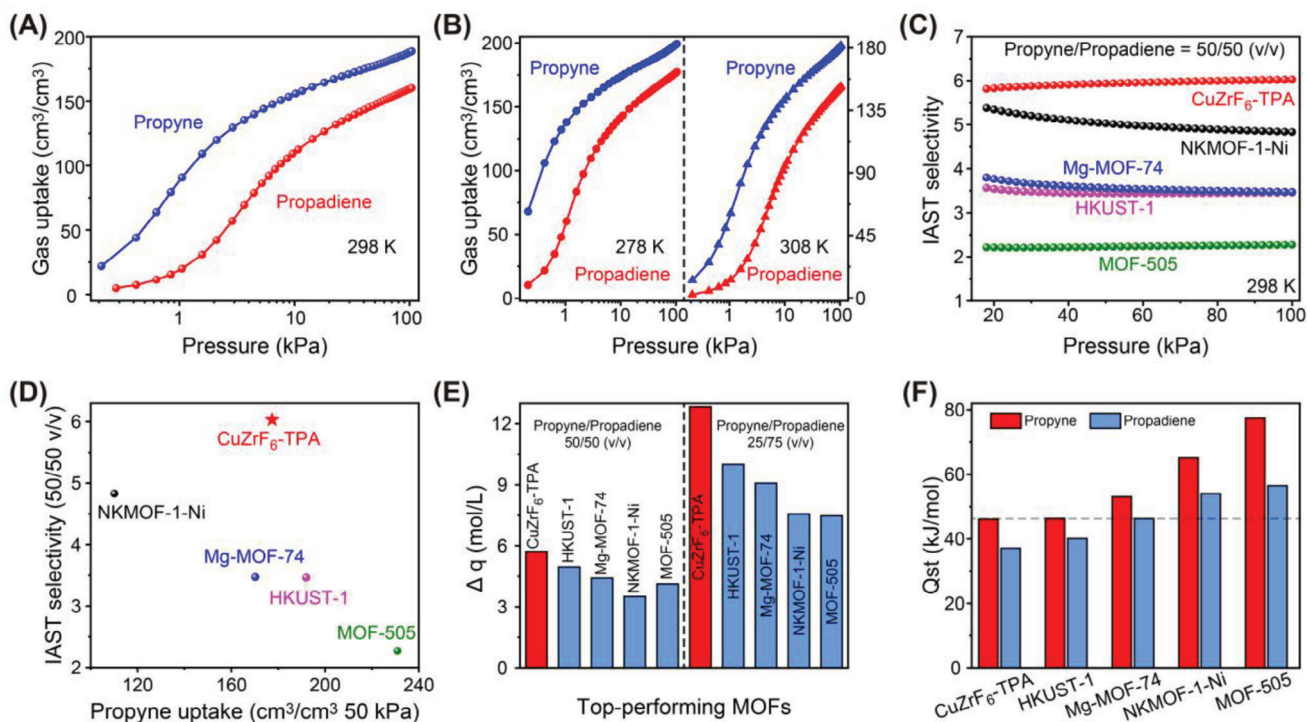
2. Results and Discussion

Blue block-shaped single crystals of CuZrF$_6$-TPA were successfully synthesized through layering a MeOH solution of TPA onto an aqueous solution of CuZrF$_6$ (**Figure 1A**). Subsequent X-ray crystal analysis unveiled that CuZrF$_6$-TPA crystallizes in a three-dimensional (3D) framework with the cubic Pm-3n space group (Table S1, Supporting Information). Every unit cell of CuZrF$_6$-TPA is composed of six Cu^{2+} cations, six ZrF$_6^{2-}$ anions and eight tridentate TPA ligands, wherein coordination-saturated Cu^{2+} is connected to four TPA nitrogen atoms and two fluorine atoms from ZrF$_6^{2-}$ anions. The capacious cage-like pore of CuZrF$_6$-TPA has a diameter of $\approx$8.5 Å (Figure 1B and Figure S2, Supporting Information), reminiscent of the characteristics observed in HKUST-1. Each pore displays twelve windows consisting of two dipyridylamine units from TPA ligands and one Cu-ZrF$_6$-Cu edge (Figure S3, Supporting Information). The window size is only of $\approx$2.6 Å after subtracting the Van der waals radii of two hydrogen atoms (Figure 1C). This specific window containing abundant Lewis basic F functional sites, aromatic surface and confined space is potential to trap propyne strongly by multiple synergistic interactions. Importantly, such window sites are distinct from the binding sites found in previous instances of AP-MOFs exhibiting linear 1D channels (e.g., SIFSIX-1-Cu, SIFSIX-3-Ni)[57,58] and thus shows promising avenues for the efficient separation of propyne/propadiene.

N$_2$ sorption test was conducted at 77 K to investigate the intrinsic porosity of CuZrF$_6$-TPA. As seen in Figure S9, Supporting Information, the N$_2$ uptake reaches rapid equilibrium at low pressures, showcasing a characteristic Type-I adsorption isotherm indicative of microporous behavior. The Brunauer-Emmett-Teller (BET) surface area and pore volume were calculated to be 1333 m^2 g^{-1} and 0.554 cm^3 g^{-1} based on the N$_2$ adsorption isotherm. Subsequently, the propyne and propadiene isotherms on CuZrF$_6$-TPA were collected at 298 K (**Figure 2A**). There are discernible differences in uptake between propyne and propadiene across the entire pressure spectrum, which is distinct from prior MOF study. At 0.5 and 1.0 bar, the propyne uptakes are 177.4 and 188.6 cm^3 cm^{-3}, surpassing those recorded for zeolites and most MOFs with robust binding sites, such as Zeolite 5A (60.1/62.4 cm^3 cm^{-3}),[70] SIFSIX-1-Cu (159.1/169.0 cm^3 cm^{-3}),[50] SIFSIX-3-Ni (102.7/107.4 cm^3 cm^{-3}),[50] UTSA-200 (111.2/113.6 cm^3 cm^{-3})[51] and NKMOF-1-Ni (110.1/128.2 cm^3 cm^{-3}),[25] and comparable with those of MOFs with open metal sites and high porosity, such as Mg-MOF-74 (170.2/186.1 cm^3 cm^{-3}),[25] HKUST-1 (192.0/206.3 cm^3 cm^{-3}),[25] and MOF-505 (230.9/245.8 cm^3 cm^{-3})[25] (Figure 2D). Then, the single-component equilibrium sorption experiments were further performed at 278 and 308 K (Figure 2B). As expected, significant disparities in propyne and propadiene uptakes persist across the entire pressure range. Notably, the adsorption capacity of propyne of CuZrF$_6$-TPA at 1 bar increases to 199.3 cm^3 cm^{-3} at 278 K.

Separation selectivity stands as a parameter of equal significance to capacity, especially when viewed within the context of real-world industry separation processes. Within this framework, the selectivities concerning a 50/50 and 25/75 v/v propyne/propadiene mixture on CuZrF$_6$-TPA were calculated using the ideal adsorbed solution theory (IAST) after fitting isotherms into dual site Langmuir equation with excellent accuracy (Table S4, Supporting Information). The IAST selectivity of CuZrF$_6$-TPA for 50/50 propyne/propadiene at 298 K is 6.0 (Figure 2C), superior to those of NKMOF-1-Ni (4.8),[25] Mg-MOF-74 (3.5),[25] HKUST-1 (3.5),[25] and MOF-505 (2.3)[25] (Figure 2D). The IAST selectivity for 25/75 propyne/propadiene mixture is also 6.0 (Figure S17, Supporting Information), which still holds the highest rank among the prominent MOFs on record – NKMOF-1-Ni (4.9), Mg-MOF-74 (3.5), HKUST-1 (3.4), and MOF-505 (2.3) (Figure S18, Supporting Information).

To comprehensively estimate the separation performance, the separation potential ($\Delta q = q_1 y_2 / y_1 - q_2$) as a combined selectivity-capacity metric introduced by Krishna first was judiciously employed here.[71] After calculating the Δq values from a
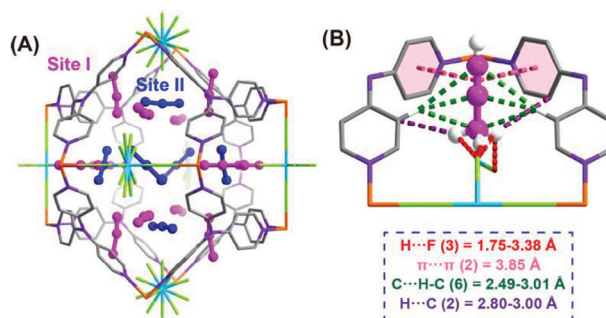
Figure 2. A) Propyne and propadiene adsorption isotherms of CuZrF$_6$-TPA at 298 K. B) Propyne and propadiene adsorption isotherms of CuZrF$_6$-TPA at 278/308 K. C) Comparison of IAST selectivity of CuZrF$_6$-TPA with other top-performing MOFs. D) Comparison of the propyne uptake at 50 kPa and IAST selectivity among top-performing MOFs. E) Comparison of separation potential of CuZrF$_6$-TPA with other top-performing MOFs. F) Comparison of the isosteric enthalpy of adsorption (Q$_{st}$) for CuZrF$_6$-TPA with other top-performing MOFs.

propyne/propadiene mixture for CuZrF$_6$-TPA and other top-performing materials, we found that the Δq values of CuZrF$_6$-TPA are the highest regardless of the propyne/propadiene ratios (Figure S21, Supporting Information). When the ratios of propyne/propadiene are 50/50 and 25/75, the Δq values of CuZrF$_6$-TPA are 5.7 and 12.8 mol L^{-1}, respectively (Figure S20, Supporting Information). Under the same conditions, the respective Δq values of HKUST-1, Mg-MOF-74, NKMOF-1-Ni and MOF-505 are only 5.0/10.0, 4.4/9.1, 3.5/7.6 and 4.1/7.5 mol L^{-1} (Figure 2E). Finally, the isosteric enthalpy of adsorption (Q$_{st}$) for CuZrF$_6$-TPA was determined by using the Clausius-Clapeyron equation. The Q$_{st}$ values at near-zero loading for propyne and propadiene are 46.1 and 37.1 kJ mol^{-1} (Figure S19, Supporting Information). It is noteworthy that these values, while moderately high, are lower than all those reported for MOFs utilized in propadiene purification, such as Mg-MOF-74 (53.1/46.3 kJ mol^{-1}),[25] NKMOF-1-Ni (65.1/54.0 kJ mol^{-1})[72] MOF-505 (77.4/56.5 kJ mol^{-1}),[25] and HKUST-1 (46.3/40.1 kJ mol^{-1}).[25] Interestingly, the gap of CuZrF$_6$-TPA between the Q$_{st}$ values for propyne and propadiene (9.0 kJ mol^{-1}) is even larger than those of HKUST-1 (6.2 kJ mol^{-1}) and Mg-MOF-74 (6.8 kJ mol^{-1}) (Figure 2F). Such moderate Q$_{st}$ values and distinguished adsorption enthalpy difference ensure both the preferential propyne adsorption and the facile regeneration of CuZrF$_6$-TPA.

To get insights into the propyne binding sites within the CuZrF$_6$-TPA structure, an experimental approach involving the introduction of propyne into the activated CuZrF$_6$-TPA was employed. Subsequent measurements were carried out using a single crystal X-ray diffractometer, which revealed a consistent framework structure within the cubic Pm-3n space group, as corroborated by Table S1, Supporting Information. Intriguingly, the adsorption capacity was determined to be 26.4 propyne molecules within an individual unit cell. This translates to approximately 4.4 propyne molecules for each ZrF$_6^{2-}$ anion, a finding that aligns seamlessly with the saturation values (4.63 propyne) obtained from single-component adsorption experiments (**Figure 3**). Two binding sites are observed for propyne: the window site is the primary site (site I, Figure 3B) that captures propyne by

Figure 3. A) Single crystal structure of propyne loaded CuZrF$_6$-TPA, revealing the major adsorption site at the windows and second adsorption site inside the pores. B) The interaction between CuZrF$_6$-TPA and propyne in adsorption site I.

2311140 (4 of 8)

ADVANCED
SCIENCE NEWS

www.advancedsciencenews.com
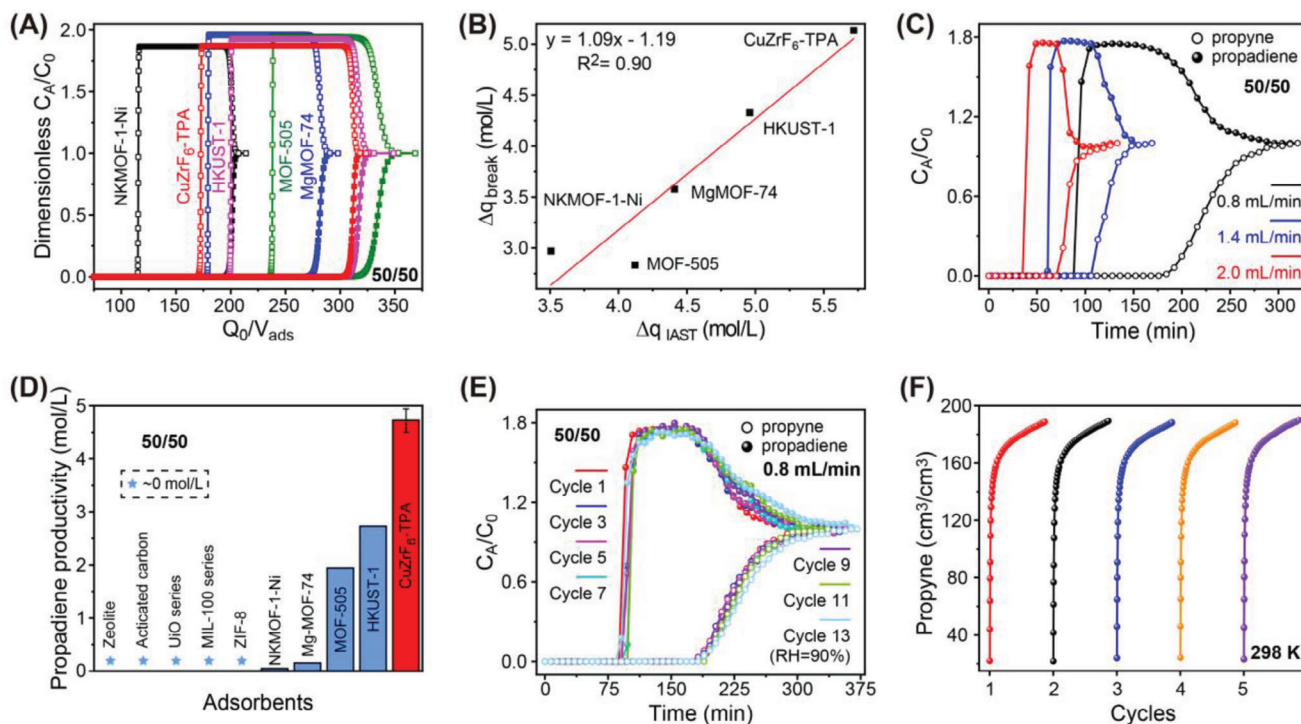
**ADVANCED
MATERIALS**

www.advmat.de

Figure 4. A) Illustration of a propyne molecule crossing the windows in $CuZrF_6$-TPA for calculating the interaction energy. B,C) Interaction energy pathway for propyne and propadiene through the windows of $CuZrF_6$-TPA. D,E) The DFT optimized adsorption configuration of propyne and propadiene in $CuZrF_6$-TPA and their respective binding energies.

multiple synergistic hydrogen bonds (C-H⋯F-Zr: 1.75-3.38 Å; C-H⋯C: 2.49-3.01 Å) and $\pi⋯\pi$ packing interaction (3.85 Å), while a secondary site exists within the large pore (site II, Figure S5, Supporting Information). The distribution ratios of propyne molecules across binding site I and II are quantified as 19.2:7.2 (Figure 3A). The binding sites of propadiene are also illustrated by single crystal X-ray diffraction and the results are discussed in Figure S6, Supporting Information.

To further understand the diffusion process in the intricate 3D interconnected channels of $CuZrF_6$-TPA, the rigid interaction energy scanning along the a axis was performed by using density functional theory (DFT) (**Figure 4A**, Tables S6 and S7, Supporting Information). The potential interaction energy of propyne or propadiene adsorbed on $CuZrF_6$-TPA was calculated as a function of the distance from the mass center of the gas molecule to the center of two windows (Figures 4B,C). As anticipated, the binding affinities exhibited considerable dependence on the positional arrangement of the gas molecules relative to the windows. The binding energy reaches maximum (-83.2 kJ mol^{-1} for propyne and -66.8 kJ mol^{-1} for propadiene) when passing through the windows. Such a large energy difference (16.4 kJ mol^{-1}) is significant enough to produce selectivity of propyne over propadiene. Specifically, propyne is tightly trapped by four C-H⋯F hydrogen bonds (2.30–2.85 Å), four C⋯H-C hydrogen bonds (2.57–2.69 Å) and two $\pi⋯\pi$ packing interactions (3.40 Å) (Figure 4D). Propadiene also interacts with the window surface by multiple hydrogen bonds and $\pi⋯\pi$ stacking, but the interaction distances are slightly longer, leading to reduced binding energy (Figure 4E).

To corroborate the dynamic separation efficacy of $CuZrF_6$-TPA for propyne/propadiene mixtures, transient breakthrough simulations were conducted. As shown in **Figure 5A** and Figure S22, Supporting Information, highly efficient separations could be accomplished by $CuZrF_6$-TPA. Notably, the time interval of $CuZrF_6$-TPA between the breakthrough of propyne and propadiene outperforms that of all other top-performing materials. The productivity of propadiene with the purity over 99.996% in a single adsorption process was further calculated for $CuZrF_6$-TPA and other materials, which showed that $CuZrF_6$-TPA has the highest productivity values of 5.1 and 11.6 mol L^{-1} from 50/50 and 25/75 propyne/propadiene mixtures, respectively. These findings align coherently with the separation potential Δq_{IAST} based on the single-component gas adsorption isotherms (Figure 5B and Figure S23, Supporting Information).

Motivated by the simulated results, experimental breakthrough studies towards equimolar propyne/propadiene mixture under different flowrates were carried out (Figure 5C). The set of three experimental breakthroughs are in quantitative agreement with the corresponding breakthrough simulations; the comparisons are provided in Figure S24, Supporting Information. In these simulations, intra-crystalline diffusional influences are considered to be of negligible importance. The conclusion to be drawn is that diffusional influence does not influence the separations with $CuZrF_6$-TPA. With a flow rate of 0.8 mL min^{-1}, propadiene was eluted at ≈96 min while propyne was not detected until ≈184 min at 298 K. The calculated experimental productivity of propadiene reached 4.8 mol L^{-1}, highly close to the simulated one (5.1 mol L^{-1}). With the flowrates increased to 1.4 and 2.0 mL min^{-1}, the elution times of the two gases shifted forward, concomitantly reducing the breakthrough

Figure 5. A) Simulated breakthrough curves of CuZrF$_6$-TPA and other top-performing materials for equimolar propyne/propadiene mixture. B) Plots of the calculated productivity of propadiene in >99.996% purity and separation potential Δq_{IAST} from equimolar propyne/propadiene mixture. C) Experimental breakthrough curves of CuZrF$_6$-TPA for equimolar propyne/propadiene mixture at 298 K with different flowrates. D) Comparison of the experimental propadiene productivity obtained by different materials from equimolar propyne/propadiene under the same conditions. E) Thirteen cycles of experimental breakthrough curves of CuZrF$_6$-TPA for equimolar propyne/propadiene at 298 K (1-12: dry condition, 13: humid condition). F) Five cycles of propyne adsorption isotherms of CuZrF$_6$-TPA at 298 K.

interval. Despite these alterations, the propadiene productivities exhibited robust consistency at 4.6 and 4.7 mol L^{-1}, respectively. This steadfastness suggests that the alteration of flow rates exerts marginal influence on the separation efficiency (Figure 5C). Aggregating data from multiple dynamic breakthrough experiments involving the 50/50 propyne/propadiene mixture across different conditions (Figures 5C,E) yielded an average calculated propadiene productivity of 4.7 mol L^{-1}, a figure surpassing previously reported benchmarks. Notably, this achievement significantly outperforms notable materials such as HKUST-1 (2.7 mol L^{-1}),[25] MOF-505 (1.9 mol L^{-1}),[25] Mg-MOF-74 (0.2 mol L^{-1})[25] and NKMOF-1-Ni (0.05 mol L^{-1})[25] (Figure 5D).

Given the pivotal role of MOF stability in industrial applications, comprehensive assessments were undertaken to evaluate the water, thermal, and cyclic stability of CuZrF$_6$-TPA. To this end, crystals of CuZrF$_6$-TPA were subjected to a week-long immersion in water. Remarkably, this treatment engendered no discernible shift in peak positions within the powder X-ray diffraction (PXRD) patterns, nor any appreciable diminishment in N$_2$ adsorption capacity at 77 K. These outcomes unequivocally affirm the structural integrity of the porous framework of CuZrF$_6$-TPA (Figures S7 and S10, Supporting Information). Thermogravimetric analysis (TGA) further underscored the robust thermal stability of the CuZrF$_6$-TPA framework, evidencing its durability even beyond 300 °C (Figure S8, Supporting Information). The exceptional cyclic stability of CuZrF$_6$-TPA was substantiated

through meticulous examination of repetitive breakthroughs and propyne adsorption cycles. Evident from Figures 5E,F, the near convergence of breakthrough curves and adsorption isotherms across twelve iterative breakthroughs and five cyclic adsorption-desorption sequences unequivocally supports the enduring stability of CuZrF$_6$-TPA. Furthermore, a comparative assessment of breakthrough experiments conducted under both dry and humid conditions (RH = 90%) accentuated the pronounced resilience of CuZrF$_6$-TPA against water vapor (Figure 5E). Besides, CuZrF$_6$-TPA can be rapidly regenerated by Ar purge at 100 °C within 2 hours (Figures S25–S28, Supporting Information).

3. Conclusions

In summary, we reported a novel ZrF$_6$$^{2-}$ anion hybrid MOF CuZrF$_6$-TPA with specific window sites for efficient propyne/propadiene separation with record propadiene productivity. The highlight of this work includes: 1) high propyne capacity of 177.4/188.6 cm^3 cm^{-3} under the pressure of 0.5 and 1 bar at 298 K; 2) benchmark separation selectivity (6.0) for equimolar propyne/propadiene mixtures; 3) the highest propyne/propadiene (50/50, 25/75) separation potential (5.7/12.8 mol L^{-1}) among the reported porous materials; 4) record high propadiene productivity (4.7 mol L^{-1}) in breakthrough experiments from equimolar propyne/propadiene mixtures; 5) ultrahigh thermal, water and recyclable stability; 6) unambiguous revealing of the specific propyne trapping sites by

**ADVANCED
SCIENCE NEWS**

www.advancedsciencenews.com

**ADVANCED
MATERIALS**

www.advmat.de

in-situ single crystal structure analysis and DFT calculation. In general, our work not only presented a new strategy to realize high-performance propyne/propadiene separation, but also demonstrated the significance of designing specific binding sites and pore features for challenging gas separation, which may also inspire the separation of other light hydrocarbon separation system.

4. Experimental Section

Preparation of CuZrF$_6$-TPA Single Crystals: To a 5 mL long thin tube was added a 1 mL of aqueous solution with CuZrF$_6$·3H$_2$O ($\approx$1.7 mg). Two milliliters of MeOH/H$_2$O mixture (v:v = 1:1) was slowly layered above the solution, followed by a 1 mL of MeOH solution of TPA ($\approx$1.0 mg). The tube was sealed and left undisturbed at 298 K. After $\approx$1 week, blue single crystals were obtained.

Bulky Synthesis of CuZrF$_6$-TPA Micro-Crystals: To a 50 mL round bottom flask was added TPA (100 mg, 0.4 mmol) and CuZrF$_6$·3H$_2$O (100 mg, 0.31 mmol). Then, 15 mL MeOH and 3 mL H$_2$O were added. The mixture was heated to 348 K and reacted for 72 h. After that, the blue micro-crystals was collected by filtration and washed by H$_2$O (10 mL $\times$ 3) and MeOH (20 mL $\times$ 3). The mass of product is over 150 mg. After complete activation, the weight was $\approx$117 mg. Yield: $\approx$63%.

Supporting Information

Supporting Information is available from the Wiley Online Library or from the author.

Conflict of Interest

The authors declare no conflict of interest.

Data Availability Statement

The data that support the findings of this study are available from the corresponding author upon reasonable request. CCDC 2280846–2280848 contains the supplementary crystallographic data for this paper. These data can be obtained free of charge from The Cambridge Crystallographic Data Centre via www.ccdc.cam.ac.uk/data_request/cif.

[1] H. V. Pham, K. N. Houk, *J. Org. Chem.* **2014**, *79*, 8968.

[2] S. Yu, S. Ma, *Angew. Chem., Int. Ed.* **2012**, *51*, 3074.

[3] T. M. V. D. Pinho e Melo, *Monatsh. Chem.* **2011**, *142*, 681.

[4] S. V. Siegar, I. Lubins, B. Breit, *ACS Catal* **2022**, *12*, 11301.

[5] E. R. H. Jones, B. L. Shaw, M. C. Whiting, *J. Am. Chem. Soc.* **1954**, *76*, 3212.

[6] N. Yoshikai, E. Nakamura, *Chem. Rev.* **2012**, *112*, 2339.

[7] Z. Gholami, F. Gholami, Z. Tišler, M. Vakili, *Energies* **2021**, *14*, 8190.

[8] R. S. Fry, J. A. Nicholls, *AIAA J.* **1974**, *12*, 1703.

[9] H. Li, J. W. Sheeran, A. M. Clausen, Y.-Q. Fang, M. M. Bio, S. Bader, *Angew. Chem., Int. Ed.* **2017**, *56*, 9425.

[10] E. E. Elboray, C. Gao, R. Grigg, *Tetrahedron* **2012**, *68*, 3103.

[11] M. Ding, R. W. Flaig, H.-L. Jiang, O. M. Yaghi, *Chem. Soc. Rev.* **2019**, *48*, 2783.

[12] B. Li, M. Chrzanowski, Y. Zhang, S. Ma, *Coordin. Chem. Rev.* **2016**, *307*, 106.

[13] H. Li, L. Li, R. Lin, W. Zhou, Z. Zhang, S. Xiang, B. Chen, *Chem* **2019**, *1*, 100006.

[14] K. Adil, Y. Belmabkhout, R. S. Pillai, A. Cadiau, P. M. Bhatt, A. H. Assen, G. Maurin, M. Eddaoudi, *Chem. Soc. Rev.* **2017**, *46*, 3402.

[15] L. Yang, S. Qian, X. Wang, X. Cui, B. Chen, H. Xing, *Chem. Soc. Rev.* **2020**, *49*, 5359.

[16] B. R. Barnett, M. I. Gonzalez, J. R. Long, *Trends Chem* **2019**, *1*, 159.

[17] X. Zhao, Y. Wang, D.-S. Li, X. Bu, P. Feng, *Adv. Mater.* **2018**, *30*, 1705189.

[18] Y. Chai, X. Han, W. Li, S. Liu, S. Yao, C. Wang, W. S. I. Da-Silva, P. Manuel, Y. Cheng, L. D. Daemen, A. J. Ramirez-Cuesta, C. C. Tang, L. Jiang, S. Yang, N. Guan, L. Li, *Science* **2020**, *368*, 1002.

[19] Y. Chen, Y. Yang, Y. Wang, Q. Xiong, J. Yang, S. Xiang, L. Li, J. Li, Z. Zhang, B. Chen, *J. Am. Chem. Soc.* **2022**, *144*, 17033.

[20] K.-J. Chen, D. G. Madden, S. Mukherjee, T. Pham, K. A. Forrest, A. Kumar, B. Space, J. Kong, Q.-Y. Zhang, M. J. Zaworotko, *Science* **2019**, *366*, 241.

[21] L. Li, L. Guo, D. H. Olson, S. Xian, Z. Zhang, Q. Yang, K. Wu, Y. Yang, Z. Bao, Q. Ren, J. Li, *Science* **2022**, *377*, 335.

[22] D.-D. Zhou, P. Chen, C. Wang, S.-S. Wang, Y. Du, H. Yan, Z.-M. Ye, C.-T. He, R.-K. Huang, Z.-W. Mo, N.-Y. Huang, J.-P. Zhang, *Nat. Mater.* **2019**, *18*, 994.

[23] G.-D. Wang, Y.-Z. Li, W.-J. Shi, L. Hou, Y.-Y. Wang, *Angew. Chem. Int. Ed.* **2023**, *62*, 202311654.

[24] Y. Wang, T. Li, L. Li, R.-B. Lin, X. Jia, Z. Chang, H.-M. Wen, X.-M. Chen, J. Li, *Adv Mater* **2023**, *35*, 2207955.

[25] Y.-L. Peng, T. Wang, C. Jin, C.-H. Deng, Y. Zhao, W. Liu, K. A. Forrest, R. Krishna, Y. Chen, T. Pham, B. Space, P. Cheng, M. J. Zaworotko, Z. Zhang, *Nat. Commun.* **2021**, *12*, 5768.

[26] M. Li, D. Li, M. O'Keeffe, O. M. Yaghi, *Chem. Rev.* **2014**, *114*, 1343.

[27] L. Yu, S. Ullah, K. Zhou, Q. Xia, H. Wang, S. Tu, J. Huang, H.-L. Xia, X.-Y. Liu, T. Thonhauser, J. Li, *J. Am. Chem. Soc.* **2022**, *144*, 3766.

[28] P.-Q. Liao, N.-Y. Haung, W.-X. Zhang, J.-P. Zhang, X.-M. Chen, *Science* **2017**, *356*, 1193.

[29] M. L. Foo, R. Matsuda, Y. Hijikata, R. Krishna, H. Sato, S. Horike, A. Hori, J. Duan, Y. Sato, Y. Kubota, M. Takata, S. Kitagawa, *J. Am. Chem. Soc.* **2016**, *138*, 3022.

[30] W. Gong, Y. Xie, X. Wang, K. O. Kirlikovali, K. B. Idrees, F. Sha, H. Xie, Y. Liu, B. Chen, Y. Cui, O. K. Farha, *J. Am. Chem. Soc.* **2023**, *145*, 2679.

[31] J. Pei, K. Shao, J.-X. Wang, H.-M. Wen, Y. Yang, Y. Cui, R. Krishna, B. Li, G. Qian, *Adv. Mater.* **2020**, *32*, 1908275.

[32] Z. Niu, X. Cui, T. Pham, G. Verma, P. C. Lan, C. Shan, H. Xing, K. A. Forrest, S. Suepaul, B. Space, A. Nafady, A. M. Al-Enizi, S. Ma, *Angew. Chem., Int. Ed.* **2021**, *60*, 5283.

[33] K. B. Idrees, Z. Li, H. Xie, K. O. Kirlikovali, M. Kazem-Rostami, X. Wang, T.-Y. Tai, T. Islamoglu, J. F. Stoddart, R. Q. Snurr, O. K. Farha, *J. Am. Chem. Soc.* **2022**, *144*, 12212.

[34] H. Yang, Y. Chen, C. Dang, A. N. Hong, P. Feng, X. Bu, *J. Am. Chem. Soc.* **2022**, *144*, 20221.

[35] J.-B. Lin, T. T. T. Nguyen, R. Vaidhyanathan, J. Burner, J. M. Taylor, H. Durekova, F. Akhtar, R. K. Mah, O. Ghaffari-Nik, S. Marx, N. Fylstra, S. S. Iremonger, K. W. Dawson, P. Sarkar, P. Hovington, A. Rajendran, T. K. Woo, G. K. H. Shimizu, *Science* **2021**, *374*, 1464.

[36] H. Zeng, M. Xie, Y.-L. Huang, Y. Zhao, X.-J. Xie, J.-P Bai, M.-Y. Wan, R. Krishna, W. Lu, D. Li, *Angew. Chem., Int. Ed.* **2019**, *58*, 8515.

[37] W. Fan, S. Yuan, W. Wang, L. Feng, X. Liu, X. Zhang, X. Wang, Z. Kang, F. Dai, D. Yuan, D. Sun, H.-C. Zhou, *J. Am. Chem. Soc.* **2020**, *142*, 8728.

[38] Y. Jiang, Y. Hu, B. Luan, L. Wang, R. Krishna, H. Ni, X. Hu, Y. Zhang, *Nat. Commun.* **2023**, *14*, 401.

[39] X. Huang, S. Jiang, D. Ma, J. Xie, X. Feng, B. Wang, *Angew. Chem., Int. Ed.* **2023**, *62*, 202303671.

[40] Z. Zhang, Y. Chen, K. Chai, C. Kang, S. B. Peh, H. Li, J. Ren, X. Shi, X. Han, C. Dejoie, S. J. Day, S. Yang, D. Zhao, *Nat. Commun.* **2023**, *14*, 3789.

[41] Y. Zhang, J. Hu, R. Krishna, L. Wang, L. Yang, X. Cui, S. Duttwyler, H. Xing, *Angew. Chem., Int. Ed.* **2020**, *59*, 17664.

[42] J.-W. Wang, S.-C. Fan, H.-P. Li, X. Bu, Y.-Y. Xue, Q.-G. Zhai, *Angew. Chem., Int. Ed.* **2023**, *62*, 202217839.

[43] X.-W. Gu, E. Wu, J.-X. Wang, H.-M. Wen, B. Chen, B. Li, G. Qian, *Sci. Adv.* **2023**, *9*, eadh0135.

[44] X. Cui, K. Chen, H. Xing, Q. Yang, R. Krishna, Z. Bao, H. Wu, W. Zhou, X. Dong, Y. Han, B. Li, Q. Ren, M. J. Zaworotko, B. Chen, *Science* **2016**, *353*, 141.

[45] Y. Zhang, W. Sun, B. Luan, J. Li, D. Luo, Y. Jiang, L. Wang, B. Chen, *Angew. Chem., Int. Ed.* **2023**, *62*, 202309925.

[46] Y.-L. Peng, T. Pham, P. Li, T. Wang, Y. Chen, K.-J. Chen, K. A. Forrest, B. Space, P. Cheng, M. J. Zaworotko, Z. Zhang, *Angew. Chem., Int. Ed.* **2018**, *57*, 10971.

[47] Y. Jiang, J. Hu, L. Wang, W. Sun, N. Xu, R. Krishna, S. Duttwyler, X. Cui, H. Xing, Y. Zhang, *Angew. Chem., Int. Ed.* **2022**, *61*, 202200947.

[48] M.-Y. Gao, A. A. Bezrukov, B.-Q. Song, M. He, S. J. Nikkhah, S.-Q. Wang, N. Kumar, S. Darwish, D. Sensharma, C. Deng, J. Li, L. Liu, R. Krishna, M. Vandichel, S. Yang, M. J. Zaworotko, *J. Am. Chem. Soc.* **2023**, *145*, 11837.

[49] T. Ke, Q. Wang, J. Shen, J. Zhou, Z. Bao, Q. Yang, Q. Ren, *Angew. Chem., Int. Ed.* **2020**, *59*, 12725.

[50] L. Yang, X. Cui, Q. Yang, S. Qian, H. Wu, Z. Bao, Z. Zhang, Q. Ren, W. Zhou, B. Chen, H. Xing, *Adv. Mater.* **2018**, *30*, 1705374.

[51] L. Li, H.-M. Wen, Chao. He, R.-B. Lin, R. Krishna, H. Wu, W. Zhou, J. Li, B. Li, B. Chen, *Angew. Chem., Int. Ed.* **2018**, *57*, 15183.

[52] H. Zeng, M. Xie, T. Wang, R.-J. Wei, X.-J. Xie, Y. Zhao, W. Lu, D. Li, *Nature* **2021**, *595*, 542.

[53] D. Liu, J. Pei, X. Zhang, X.-W. Gu, H.-M. Wen, B. Chen, G. Qian, B. Li, *Angew. Chem., Int. Ed.* **2023**, *62*, 202218590.

[54] Y. Xie, Y. Shi, E. M. Cedeño Morales, A. E. Karch, B. Wang, H. Arman, K. Tan, B. Chen, *J. Am. Chem. Soc.* **2023**, *145*, 2386.

[55] A. Cadiau, K. Adil, P. M. Bhatt, Y. Belmabkhout, M. Eddaoudi, *Science* **2016**, *353*, 137.

[56] Q. Dong, Y. Huang, J. Wan, Z. Lu, Z. Wang, C. Gu, J. Duan, J. Bai, *J. Am. Chem. Soc.* **2023**, *145*, 8043.

[57] S. Noro, R. Kitaura, M. Kondo, S. Kitagawa, T. Ishii, H. Matsuzaka, M. Yamashita, *J. Am. Chem. Soc.* **2002**, *124*, 2568.

[58] O. Shekhah, Y. Belmabkhout, K. Adil, P. M. Bhatt, A. J. Cairns, M. Eddaoudi, *Chem. Commun.* **2015**, *51*, 13595.

[59] L. Wang, W. Sun, Y. Zhang, N. Xu, R. Krishna, J. Hu, Y. Jiang, Y. He, H. Xing, *Angew. Chem., Int. Ed.* **2021**, *60*, 22865.

[60] P. Zhang, Y. Zhong, Y. Zhang, Z. Zhu, Y. Liu, Y. Su, J. Chen, S. Chen, Z. Zeng, H. Xing, S. Deng, J. Wang, *Sci. Adv.* **2022**, *8*, eabn9231.

[61] H. Li, C. Liu, C. Chen, Z. Di, D. Yuan, J. Pang, W. Wei, M. Wu, M. Hong, *Angew. Chem., Int. Ed.* **2021**, *60*, 7547.

[62] L. Yang, X. Cui, Z. Zhang, Q. Yang, Z. Bao, Q. Ren, H. Xing, *Angew. Chem., Int. Ed.* **2018**, *57*, 13145.

[63] Q.-L. Qian, X.-W. Gu, J. Pei, H.-M. Wen, H. Wu, W. Zhou, B. Li, G. Qian, *J. Mater. Chem. A* **2021**, *9*, 9248.

[64] Y. Belmabkhout, P. M. Bhatt, K. Adil, R. S. Pillai, A. Cadiau, A. Shkurenko, G. Maurin, G. Liu, W. J. Koros, M. Eddaoudi, *Nat. Energy* **2018**, *3*, 1059.

[65] J. Wang, Y. Zhang, Y. Su, X. Liu, P. Zhang, R.-B. Lin, S. Chen, Q. Deng, Z. Zeng, S. Deng, B. Chen, *Nat. Commun.* **2022**, *13*, 200.

[66] Y. Hu, Y. Jiang, J. Li, L. Wang, M. Steiner, R. F. Neumann, B. Luan, Y. Zhang, *Adv. Funct. Mater.* **2023**, *33*, 2213915.

[67] F. Zheng, L. Guo, R. Chen, L. Chen, Z. Zhang, Q. Yang, Y. Yang, B. Su, Q. Ren, Z. Bao, *Angew. Chem., Int. Ed.* **2022**, *61*, 202116686.

[68] Y. Zhang, L. Yang, L. Wang, S. Duttwyler, H. Xing, *Angew. Chem., Int. Ed.* **2019**, *58*, 8145.

[69] Z. Zhang, Q. Yang, X. Cui, L. Yang, Z. Bao, Q. Ren, H. Xing, *Angew. Chem., Int. Ed.* **2017**, *56*, 16282.

[70] C. He, R. Krishna, Y. Chen, J. Yang, J. Li, L. Li, *Chinese J. Chem. Eng.* **2021**, *37*, 217.

[71] R. Krishna, *RSC Adv.* **2017**, *7*, 35724.

[72] Y.-L. Peng, C. He, T. Pham, T. Wang, P. Li, R. Krishna, K. A. Forrest, A. Hogan, S. Shanelle, B. Space, M. Fang, Y. Chen, M. J. Zaworotko, J. Li, L. Li, Z. Zhang, P. Cheng, B. Chen, *Angew. Chem., Int. Ed.* **2019**, *58*, 10209.

ADVANCED MATERIALS

Supporting Information

Specific Propyne Trapping Sites within a Robust MOF for Efficient Propyne/Propadiene Separation with Record Propadiene Productivity

Yunjia Jiang, Lingyao Wang, Jianbo Hu, Rajamani Krishna, Banglin Chen* and Yuanbin Zhang*

Specific Propyne Trapping Sites within a Robust MOF for Efficient Propyne/Propadiene Separation with Record Propadiene Productivity

Yunjia Jiang, Lingyao Wang, Jianbo Hu, Rajamani Krishna, Banglin Chen,* Yuanbin Zhang*

Y. Jiang, L. Wang, B. Chen, Y. Zhang

Key Laboratory of the Ministry of Education for Advanced Catalysis Materials, College of Chemistry and Life Sciences, Zhejiang Normal University, Jinhua 321004, China.

E-mail: ybzhang@zjnu.edu.cn

J. Hu

Zhejiang Lab, Hangzhou, 311100, P.R. China.

R. Krishna

Van't Hoff Institute for Molecular Sciences, University of Amsterdam, Science Park 904, 1098 XH Amsterdam, Netherlands.

B. Chen

Fujian Provincial Key Laboratory of Polymer Materials, College of Chemistry & Materials Science, Fujian Normal University, Fuzhou 350007, P.R. China.

E-mail: banglin.chen@fjnu.edu.cn

I   General Information and Procedures

Unless otherwise noted, all the reactions were performed under air without N_2 or Ar protection. All reagents were used as received without purification unless stated otherwise.

Chemicals: Tri(pyridin-4-yl)amine (TPA, 99%) was purchased from Tensus Biotech Company. The purity of all organic compounds was identified by ^{1}H NMR and ^{13}C{^{1}H} NMR. CuO (99%) and ZrO_2 (99%) were purchased from Energy Chemical. HF ($\geq$ 40%) was purchased from Greagent. Propyne (99.9%), propadiene (99.9%), propyne/propadiene (50:50), N_2 (99.9999%), He (99.9999%), Ar (99.9999%) were purchased from Datong Co., Ltd. All other reagents were used without further purification.

Preparation of CuZrF$_6$·3H$_2$O: CuO (1.5 g, 19 mmol, 1 eq), ZrO_2 (2.3 g, 19 mmol, 1 eq) and HF (aq, 40%, 5.0 mL, 6 eq) were added to a 50 mL Teflon lined stainless autoclave. The mixture was heated at 60 °C for 24 h. After that the mixture was cooled to room temperature and a clear blue aqueous $CuZrF_6$ solution was obtained with a small amount of unreacted CuO black solid in the bottom. After removing the solid by centrifugation, the blue aqueous solution was evaporated at 100 °C for more than 5 h in an oil bath, yielding the blue crystalline powder of CuZrF$_6$·3H$_2$O (3.7 g, 71.7% based on CuO).

Preparation of CuZrF$_6$-TPA single crystals: To a 5 mL long thin tube was added a 1 mL of aqueous solution with CuZrF$_6$·3H$_2$O (~1.7 mg). 2 mL of MeOH/H$_2$O mixture (v:v=1:1) was slowly layered above the solution, followed by a 1 mL of MeOH solution of TPA (~1.0 mg). The tube was sealed and left undisturbed at 298 K. After ~1 week, blue single crystals were obtained. Anal. Cal (%) for $Cu_6Zr_6F_{36}C_{150}H_{234}N_{32}O_{39}$ ([$Cu_6(TPA)_4(ZrF_6)_6$·30CH$_3$OH·9H$_2$O]): C, 38.12; H, 4.96; N, 9.49. Found: C, 38.34; H, 5.22; N, 9.76.

Bulky synthesis of CuZrF$_6$-TPA micro-crystals: To a 50 mL round bottom flask was added TPA (100 mg, 0.4 mmol) and CuZrF$_6$·3H$_2$O (100 mg, 0.31 mmol). Then 15 mL MeOH and 3 mL H$_2$O were added. The mixture was heated to 348 K and reacted for 72 h. After that, the blue micro-crystals was collected by filtration and washed by H$_2$O (10 mL × 3) and MeOH (20 mL × 3). The mass of product is over 150 mg. After complete activation, the weight was ~117 mg. Yield: ~63%.

Preparation of gas loaded CuZrF$_6$-TPA: The synthesized CuZrF$_6$-TPA was filled into a glass tube and activated at 120 °C for 12 h. After the sample cooling down, the propyne or propadiene was induced into the sample respectively with Builder SSA 7000 (Beijing) instrument until the pressure reach to 1 bar at 298 K and maintain the state for another hour. Then, the tube was sealed. Finally, the crystals were picked out and covered with the degassed oil, and single crystal X-ray diffraction measurements were carried out at 298 K as soon as possible.

Single-crystal X-ray diffraction studies were conducted at 152 K or 120 K on the Bruker D8 VENTURE diffractometer equipped with a PHOTON-II detector (MoKα, λ = 0.71073 Å). Indexing was performed using APEX2. Data integration and reduction were completed using SaintPlus 6.01. Absorption correction was performed by the multi-scan method implemented in SADABS. The space group was determined using XPREP implemented in APEX2. The structure was solved with SHELXS-97 (direct methods) and refined on F2 (nonlinear least-squares method) with SHELXL-97 contained in APEX2, WinGX v1.70.01, and OLEX2 v1.1.5 program packages. All non-hydrogen atoms were refined anisotropically. The contribution of disordered solvent molecules was treated as diffuse using the Squeeze routine implemented in Platon.

Powder X-ray diffraction (PXRD) data were collected on the SHIMADZU XRD-6000 diffractometer (Cu Kαλ = 1.540598 Å) with an operating power of 40 KV, 30 mA and a scan speed of 4.0°/min. The range of 2θ was from 5° to 50°.

Thermal gravimetric analysis was performed on the TGA STA449F5 instrument. Experiments were carried out using a platinum pan under nitrogen atmosphere which conducted by a flow rate of 60 mL/min nitrogen gas. First, the samples were heated at 80 °C for 2 h to remove the water residue and equilibrated for 5 minutes, then cooled down to 50 °C. The data were collected at the temperature range of 50 °C to 600 °C with a ramp of 10 °C /min.

The element analysis was performed on a Vario EL cube elemental analyzer (ELEMENTAR, Vario EL Cube, Germany). In detail, about 5 mg samples which are as-synthesized were weighed and wrapped in a tin foil ark, then placed in the sample tray. Using high-purity helium as the carried gas, the content of each element was detected by a TCD detector in C, H and N mode, respectively.

The static gas adsorption equilibrium measurements were performed on the Builder SSA 7000 (Beijing) instrument. Before gas adsorption measurements, the sample of $CuZrF_6$-TPA (~100 mg) were evacuated at 25 ºC for 2 h firstly, and then at 120 ºC for 10 h until the pressure dropped below 7 μmHg. The sorption isotherms were collected at 77, 278, 298 and 308 K on activated samples.The experimental temperatures were controlled by liquid nitrogen bath (77 K)and water bath (278-308 K), respectively.

Fitting of experimental data on pure component isotherms

The unary isotherm data for propyne, and propadiene, measured at three different temperatures 278 K, 298 K, and 308 K in $CuZrF_6$-TPA were fitted with excellent accuracy using the dual-site Langmuir model, where we distinguish two distinct adsorption sites A and B:

S1: $q = \frac{q_{sat,A}b_A p}{1+b_A p} + \frac{q_{sat,B}b_B p}{1+b_B p}$

In eq (S1), the Langmuir- parameters b_A, b_B are both temperature dependent

S2: $b_A = b_{A0}\, exp\left(\frac{E_A}{RT}\right);\ b_b = b_{B0}\, exp\left(\frac{E_B}{RT}\right)$

In eq (S2), E_A, E_B are the energy parameters associated with sites A, and B, respectively.

The fit parameters are provided in Table S4.

Isosteric heat of adsorption

The isosteric heat of adsorption, Q_{st}, is defined as

$$Q_{st} = -RT^2\left(\frac{\partial \ln p}{\partial T}\right)_q \tag{S3}$$

where the derivative in the right member of eq (S3) is determined at constant adsorbate loading, q. The derivative was determined by analytic differentiation of the combination of eq (S1), eq (S2), and eq (S3).

IAST selectivities and separation potential

A key metric that quantifies the efficacy of a microporous adsorbent for separation of a binary mixture is the adsorption selectivity, S_{ads}, defined by

$$S_{ads} = \frac{q_1/q_2}{p_1/p_2} \tag{S4}$$

where q_1 and q_2 are the molar loadings of the guest components in the adsorbed phase in equilibrium with a bulk gas phase mixture with partial pressures p_1 and p_2. The mixture adsorption equilibrium is commonly determined using the Ideal Adsorbed Solution theory (IAST)[1] using fits of unary isotherms as input data.

These mixture separations are envisaged to be carried out in fixed bed adsorbers. In such devices, the separations are dictated by a combination of adsorption selectivity and uptake capacity. Using the shock wave model for fixed bed adsorbers, Krishna[2, 3] has suggested that the appropriate metric is the separation potential, Δq_1.

$$\Delta q = q_1 \frac{y_{20}}{y_{10}} - q_2 \tag{S5}$$

In eq (S5) y_{10}, y_{20} are the mole fractions of the feed mixture during the adsorption cycle. In the derivation of eq (S5), it is assumed that the concentration "fronts" traversed the column in the form of shock waves during the desorption cycle. The molar loadings q_1, q_2 of the two components are determined using the Ideal Adsorbed Solution Theory (IAST) of Myers and Prausnitz using the unary isotherm fits as data inputs.[1] The physical significance of Δq is the maximum productivity of pure propadiene(2) that is achievable in the adsorption cycle of PSA operations.

The IAST calculations of S_{ads}, and Δq were performed for binary 50/50 propyne(1)/propadiene(2) and 25/75 propyne(1)/propadiene(2) mixtures at 298 K, at total pressures ranging from 1 to 100 kPa. The values for CuZrF$_6$-TPA were compared with those for HKUST-1, MgMOF-74, NKMOF-1-Ni, and MOF-505 using the published data on unary isotherm fits from Peng et al.[4]

We also performed IAST calculations of S_{ads}, and Δq were performed for binary propyne(1)/propadiene(2) mixtures at 298 K, at 100 kPa with varying mole fractions y_1 of propyne(1) in the feed mixture.

Transient breakthrough simulations

Transient breakthrough simulations were carried out using the methodology described in earlier publications.[2, 3, 5-7] In these simulations, intra-crystalline diffusion influences are ignored.

The simulations were performed in a fixed bed with the following parameters: adsorber length, L = 0.3 m; cross-sectional area, A = 1 m^2; interstitial gas velocity in the bed, v = 0.1 m s^{-1}; voidage of the packed bed, = 0.4; the superficial gas velocity at the inlet to the bed, u_0 = 0.04 m s^{-1}. The volumetric flow rate of the gas mixture at the inlet Q_0 = 40 L s^{-1}. The volume of MOF used in the simulations is

$V_{ads} = LA(1-\varepsilon)$ = 0.18 m^3. Also, note that since the superficial gas velocity is specified, the specification of the cross-sectional area of the tube, A, is not relevant in

the simulation results presented; essentially, we set A = 1 m². The total volume of the bed is $V_{bed} = LA$. It is important to note that the volume of adsorbent, V_{ads}, includes the pore volume of the adsorbent material. If   is the framework density, the mass of the adsorbent in the bed is $m_{ads} = (1-\varepsilon) \times (L \text{ m}) \times (A \text{ m}^2) \times (\rho \text{ kg m}^{-3})$ kg. In these breakthrough simulations we use the same volume of adsorbent in the breakthrough apparatus, i.e. $(1-\varepsilon) \times A \times L$ = 0.18 m³ = 180 L.

The mixture adsorption equilibrium were determined using the Ideal Adsorbed Solution Theory (IAST) of Myers and Prausnitz;[1] the unary isotherm data used are based on molecular simulations.

The breakthrough data are presented in terms of the dimensionless concentrations at the exit of the fixed bed, c_i/c_{i0}, as function of the modified time parameter

$$\frac{(Q_0 = \text{flow rate L s}^{-1}) \times (\text{time in s})}{(\text{kg MOF packed in tube})} = \frac{Q_0 t}{m_{ads}} = \text{L kg}^{-1}.$$

Transient breakthrough experiments were performed for binary 50/50 propyne(1)/propadiene(2), and 25/75 propyne(1)/propadiene(2) mixtures at 298 K, at total pressure of 100 kPa. From the simulations, the productivities of purified propadiene(2), containing less than 1000 ppm propyne(1), were determined from a material balance. For the five different MOFs CuZrF6-TPA, HKUST-1, MgMOF-74, NKMOF-1-Ni, and MOF-505 the productivities of purified propadiene(2) from breakthrough simulations are compared with the corresponding IAST values of the separation potential Δq; the inter-relations in nearly line. The actual productivities from breakthrough simulations are lower than the corresponding Δq values.

1. Myers, A. L.; Prausnitz, J. M. Thermodynamics of Mixed Gas Adsorption. *A.I.Ch.E.J.* **1965**, *11*, 121-130.
2. Krishna, R. Screening Metal-Organic Frameworks for Mixture Separations in Fixed-Bed Adsorbers using a Combined Selectivity/Capacity Metric. *RSC Adv.* **2017**, *7*, 35724-35737. https://doi.org/10.1039/C7RA07363A.
3. Krishna, R. Metrics for Evaluation and Screening of Metal-Organic Frameworks for Applications in Mixture Separations. *ACS Omega* **2020**, *5*, 16987−17004.

https://doi.org/10.1021/acsomega.0c02218.

4.　Peng, Y.-L.; Wang, T.; Jin, C.; Deng, C.-H.; Zhao, Y.; Liu, W.; Forrest, K. A.; Krishna, R.; Chen, Y.; Pham, T.; Space, B.; Cheng, P.; Zaworotko, M. J.; Zhang, Z. Efficient Propyne/Propadiene Separation by Microporous Crystalline Physiadsorbents. *Nat. Commun.* **2021**, *12*, 5768. https://doi.org/10.1038/s41467-021-25980-y.

5.　Krishna, R. The Maxwell-Stefan Description of Mixture Diffusion in Nanoporous Crystalline Materials. *Microporous Mesoporous Mater.* **2014**, *185*, 30-50. https://doi.org/10.1016/j.micromeso.2013.10.026.

6.　Krishna, R. Methodologies for Evaluation of Metal-Organic Frameworks in Separation Applications. *RSC Adv.* **2015**, *5*, 52269-52295. https://doi.org/10.1039/C5RA07830J.

7.　Krishna, R. Methodologies for Screening and Selection of Crystalline Microporous Materials in Mixture Separations. *Sep. Purif. Technol.* **2018**, *194*, 281-300. https://doi.org/10.1016/j.seppur.2017.11.056.

Breakthrough experiments

The breakthrough experiments were carried out in the dynamic gas breakthrough equipment HP-MC41. The experiments were conducted using a stainless steel column (dimensions: 4.6 mm inner diameter × 50 mm length). The weight of $CuZrF_6$-TPA packed in the columns was 0.57 g. The column packed with sample was first purged with a Ar flow (5 mL min^{-1}) for 18 h at 120 °C. The mixed gases of propyne/propadiene (v/v, 50/50), propyne/propadiene/propylene (v/v, 5/5/90) and propyne/propadiene (v/v, 2.5/2.5/90) were then introduced. Outlet gas from the column was monitored using gas chromatography (GC-9860-5CNJ) with the thermal conductivity detector TCD.

The breakthrough experiments under the humid conditions were conducted as shown in Figure S1B. At the beginning, the gas mixture of propyne/propadiene (v/v, 50:50, 0.8 mL/min) was introduced to the bubbler full of water, after the state reached equilibrium, the gas mixture was further introduced into the column packed with activated sample. Outlet gas from the column was monitored using gas chromatography (GC-9860-5CNJ) with the thermal conductivity detector TCD.

The illustration of the gas breakthrough equipment working mechanism is showing as below: A-B) under work; C) under purge; D) under vacuum.

Figure S1. The illustration of the gas breakthrough equipment working mechanism containing gas pipelines, pressure gauge, flowmeter, hygrometer, GC, bubbler and pump: A) under work in dry conditions; B) under work in humid conditions; C) under purge; D) under vacuum.

Density functional theory (DFT) calculations

The diffusion potential energies of propyne and propadiene through the windows were calculated by relaxed scan calculations. In the scan calculations, the C atoms of propyne and propadiene were held fixed the H atoms were keep relaxed. All of the density function theory (DFT) calculations were performed by Castep package. The generalized gradient approximation (GGA) with Perdew–Burke–Ernzerhof (PBE) exchange correlation were used in the DFT calculations. A semi-empirical addition of dispersive forces to conventional DFT was included in the calculation to account for van der Waals interactions. The cutoff energy was set as 544 ev and the k-point set was $2 \times 2 \times 2$. The equation for the calculation of binding energy (ΔE) is defined as: $\Delta E = E(MOF) + E(gas) - E(MOF+gas)$
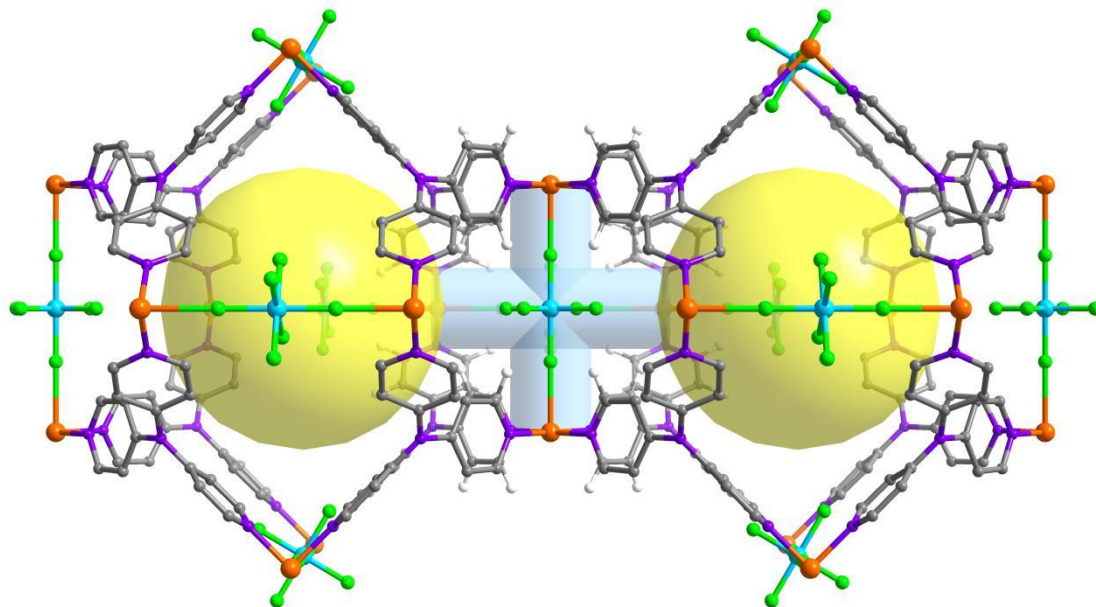
Figure S2. Structure of CuZrF$_6$-TPA.
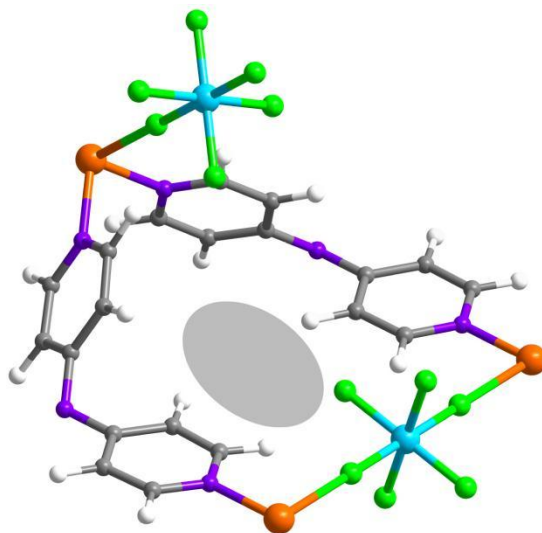
Figure S3. The window shared by large pore and small pore in CuZrF$_6$-TPA.

Table S1. Single crystal data of as synthesized $CuZrF_6$-TPA, $CuZrF_6$-TPA·C_3H_4 (Propyne), $CuZrF_6$-TPA·C_3H_4 (Propadiene).

		$CuZrF_6$-TPA as synthesized	$CuZrF_6$-TPA·C_3H_4 (Propyne)	$CuZrF_6$-TPA·C_3H_4 (Propadiene)
cell	a=b=c	17.6288(5)	17.607(5)	17.6117(4)
	α=β=γ	90	90	90
Temperature		152	120	120
Space group		Pm-3n	Pm-3n	Pm-3n
Hall group		-P 4n 2 3	-P 4n 2 3	-P 4n 2 3
Formula		$CuZrF_6C_{20}H_{16}N_{5.33}$	$(CuZrF_6C_{20}H_{16}N_{5.33})$ ·3.2(C_3H_4) 1.2(C_3) 2.293(O)	$(CuZrF_6C_{20}H_{16}N_{5.33})$ ·3.8(C_3H_4) 3.28(H_2O)
MW		599.81	807.11	790.74
density		1.091	1.473	1.442
Z		6	6	6
Data completeness		0.999	1.002	0.993
R		0.0550(844)	0.0720	0.0550(730)
wR2		0.1773(1158)	0.2430(1030)	0.2604(890)
S		1.077	1.074	1.107
CCDC. No		2280848	2280846	2280847
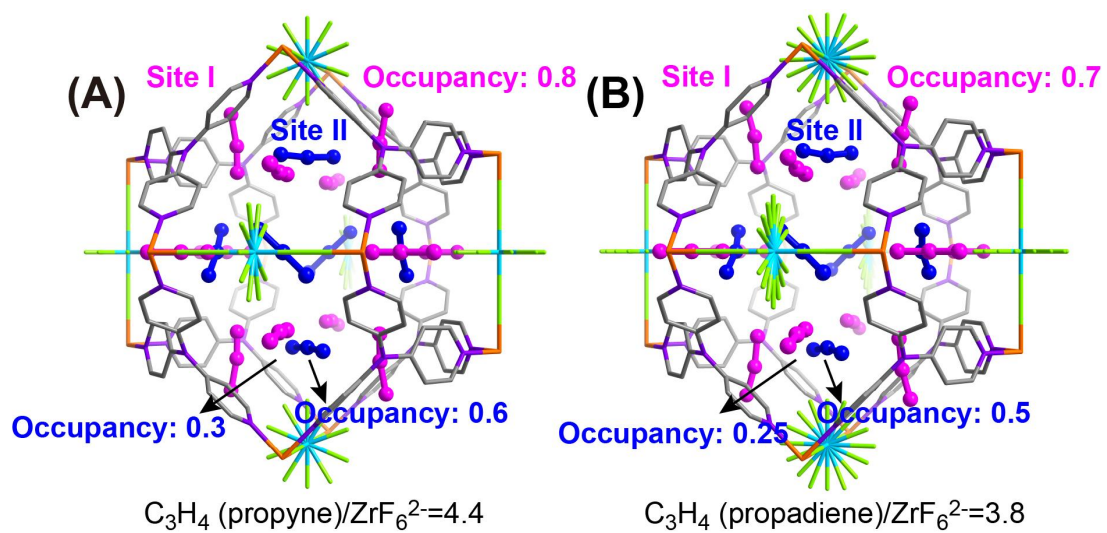
Figure S4. Single crystal structure of (A) C_3H_4 (propyne) loaded CuZrF$_6$-TPA and (B) C_3H_4 (propadiene) loaded CuZrF$_6$-TPA.
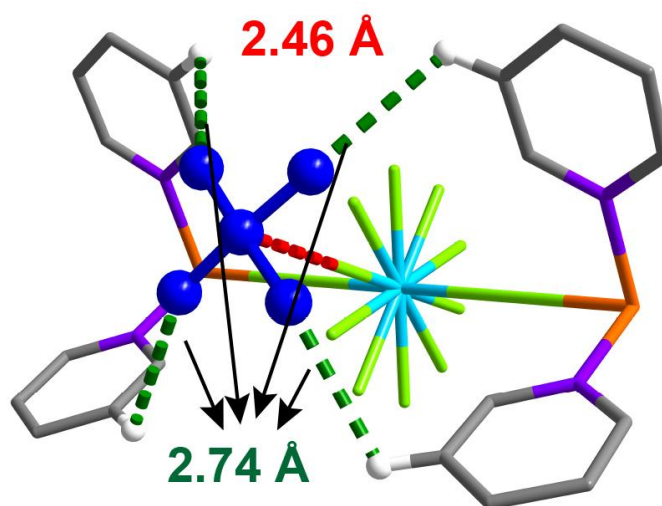
Figure S5. Binding site II of propyne

(A)

H⋯F (2) = 1.86-3.28 Å
π⋯π (4) = 3.84-3.97 Å
C⋯H-C (6) = 2.49-3.01 Å

(B)

2.43 Å

2.85 Å
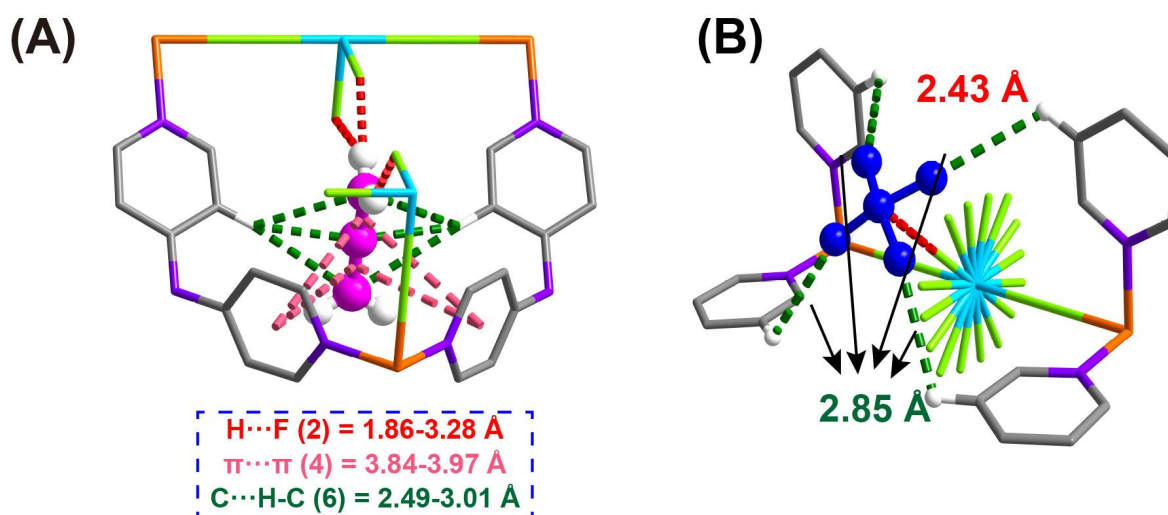
Figure S6. Binding site I (A) and II (B) of propadiene.

The propadiene loaded crystal is still in the cubic Pm-3n space group, and 22.8 propadiene molecules can be adsorbed in each unit cell, equaling 3.8 molecules for each anion, which is consistent with the saturated values from single-component adsorption tests (3.9 propadiene molecules/ZrF_6^{2-} anion). There are two binding sites for propadiene: the major site is the window site, propadiene molecule is adsorbed by C-H⋯F bonds (1.60 and 2,74 Å), π⋯π packing interaction (3.84-3.97 Å) and multiple van der Waals interations (2.49-3.01 Å); the secondary binding site is in the large pore, and the ratios of propadiene distributed in site I and II is 16.8/6.0.

Table S2. Element analysis of CuZrF$_6$-TPA.

	Elemental	N	C	H	C/N	C/H
% (mass)	Found	9.76	38.34	5.22	3.93	7.34
	Cal.	9.49	38.12	4.96	4.01	7.68
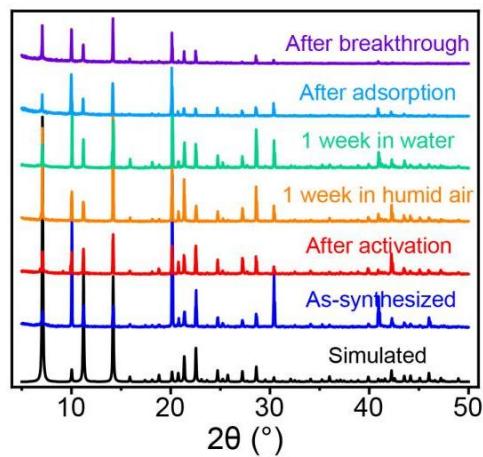
Figure S7. PXRD patterns of CuZrF$_6$-TPA after different treatment.
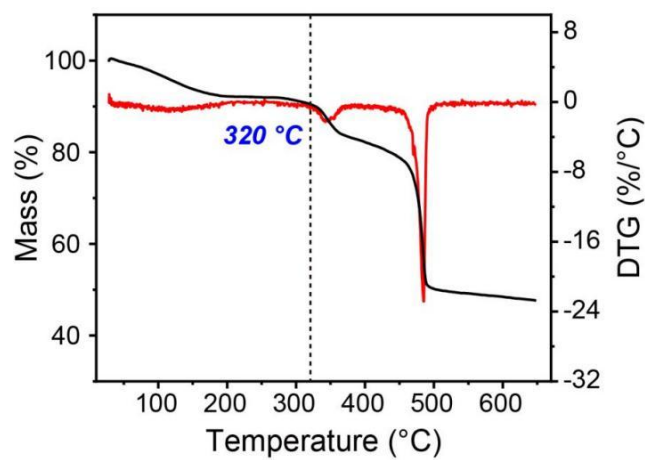
Figure S8. TGA and DTG curves of CuZrF$_6$-TPA. The weight loss before 150 ºC is because of the loss of MeOH and water from the sample. The weight keeps consistent until ~320 ºC.

III Adsorption data, Selectivity and Q_{st}
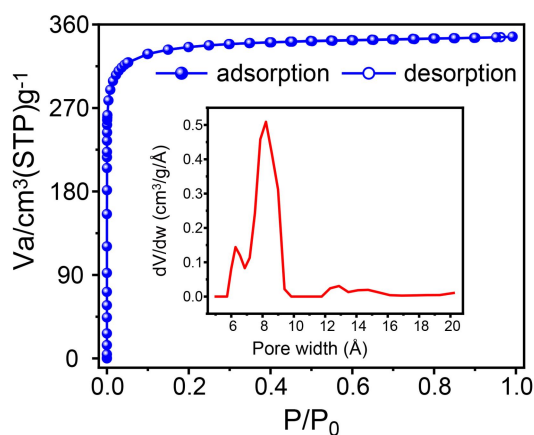
Figure S9. 77 K N_2 adsorption isotherms of CuZrF$_6$-TPA and its calculated pore size distribution (inset).

The BET surface area calculated from the N_2 adsorption isotherms under the pressure range of P/P$_0$ = 0.01-0.05 (for micropores) is 1333 m^2/g.

MBET summary:

Slope = 2.612;

Intercept = 1.214× 10^{-3};

Correlation coefficient, r= 0.999978;

C constant = 2153.371

The total pore volume calculated from the N_2 adsorption isotherms is 0.554 cm^3/g.
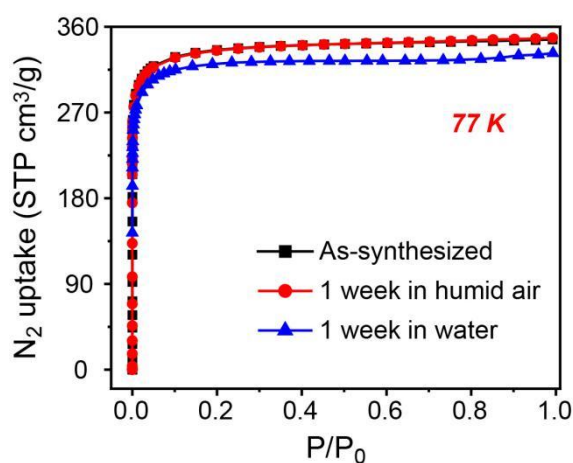
Figure S10. The adsorption isotherms of N_2 at 77 K on as-synthesized CuZrF$_6$-TPA, and CuZrF$_6$-TPA after exposure in air or soak in water for 1 week.
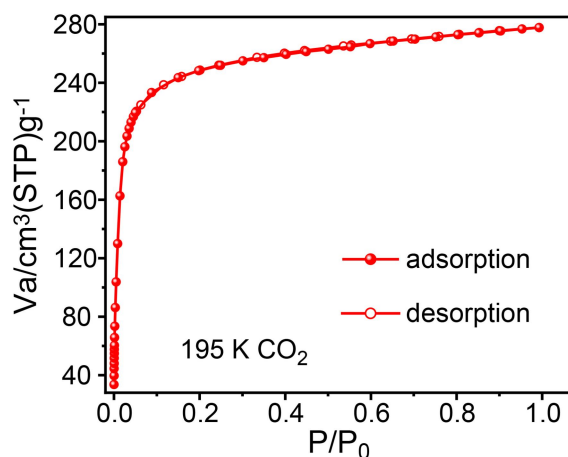
Figure S11. The sorption isotherms of CO_2 on CuZrF$_6$-TPA at 195 K.
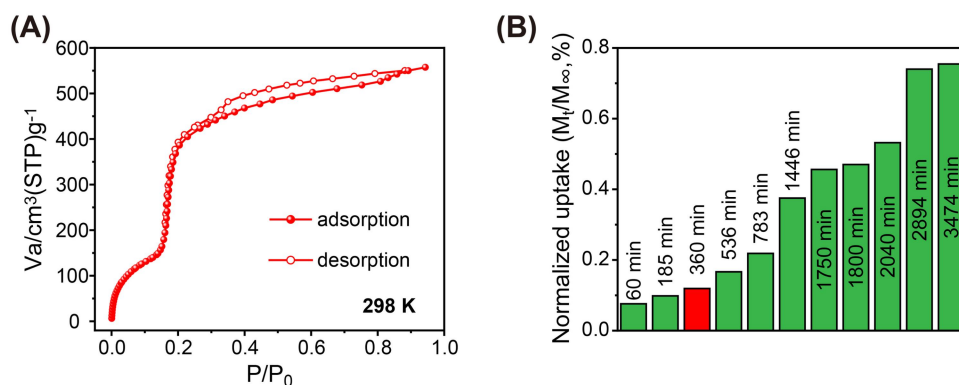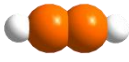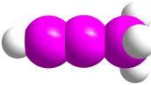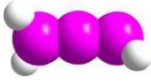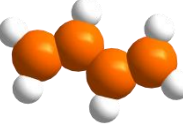
Figure S12. (A) H_2O sorption isotherms of CuZrF$_6$-TPA at 298 K. (B) Time related H_2O uptake in breakthrough experiments (N_2, RH=100%) at 298 K. Flow rate: 5 mL/min.

Experimental method: The column packed with CuZrF$_6$-TPA was activated completely firstly, and then N_2 with saturated moisture was introduced at a flow rate of 5 mL/min. After each period, the column was picked out and weighted by an analytical balance to calculate the adsorbed amount of water. The adsorbed N_2 amount is neglected.

As shown in Figure S12A, the saturated H_2O uptake of CuZrF$_6$-TPA is 557.36 cm^3/g (448.25 mg/g). However, the adsorption rate is quite low,. After six hours, the the normalized uptake is just 11.9% of saturated uptake (Figure S12B).

Table S3 Comparison of propyne and propadiene.

Gas molecules	Gas molecules	Kinetic Diameter (Å)	Molecular size (Å^3)	Boiling point (K)	Polarizability (×10^{-25} cm^3)
C_2H_2		3.3	3.32 × 3.34 × 5.70	188.4	33.3-39.3
C_2H_4		4.16	3.28 × 4.18 × 4.84	169.45	42.5
C_2H_6		4.44	3.81 × 4.08 × 4.82	184.6	44.3-44.7
C_3H_4 (propyne)		4.2	4.16 × 4.01 × 6.51	249.95	55.5
C_3H_4 (propadiene)		4.0	3.71 × 3.71 × 6.13	239	56.9
C_3H_6		4.68	4.65 × 4.16 × 6.44	225.45	62.6
C_3H_8		4.3-5.11	4.20 × 4.60 × 6.80	231.05	62.9-63.7
1,3-butadiene		4.24	3.40 × 5.36 × 7.84	268.3	7.62
n-C_4H_8		4.85	4.05 × 4.17 × 7.87	266.9	7.54
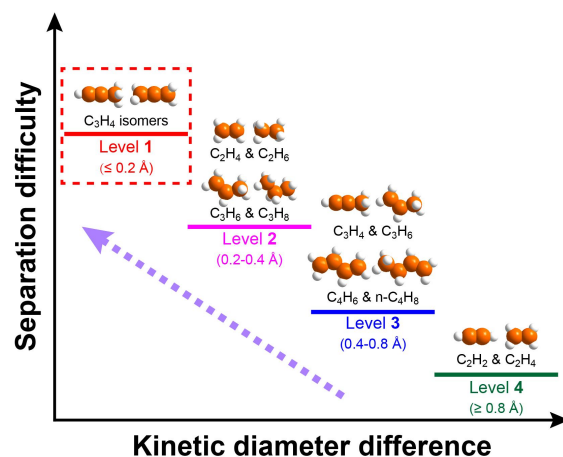
Figure S13. The complexity of different hydrocarbon separation systems classified by the molecular size difference.
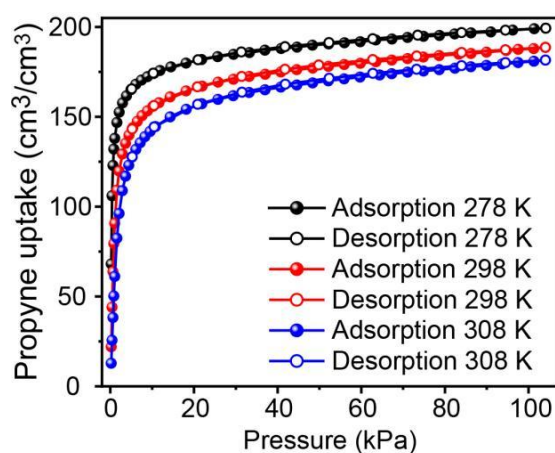
Figure S14. The sorption isotherms of C_3H_4 (propyne) on CuZrF$_6$-TPA at 278, 298, and 308 K.
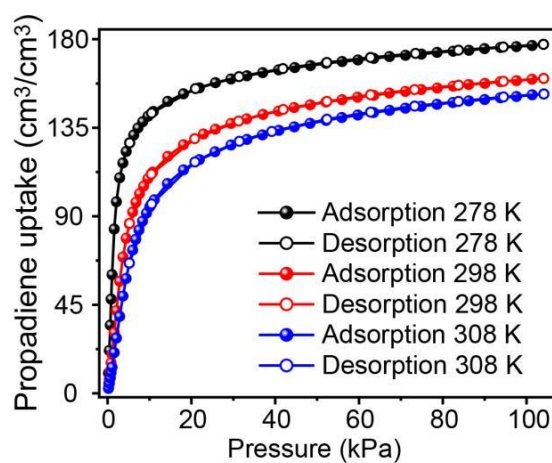
Figure S15. The sorption isotherms of C_3H_4 (propadiene) on CuZrF$_6$-TPA at 278, 298, and 308 K.

Table S4. Dual-site Langmuir fits for propyne, and propadiene in CuZrF$_6$-TPA.

	Site A			Site A		
	$q_{A, sat}$ cm^3/g	b_{A0} Pa^{-1}	E_A J/mol	$q_{B, sat}$ cm^3/g	b_{B0} Pa^{-1}	E_B J/mol
propyne	154.23	8.32E-09	46136.45	38.50	1.46E-09	38573.60
propadiene	34.83	5.35E-18	80751.33	148.51	6.44E-08	37055.94
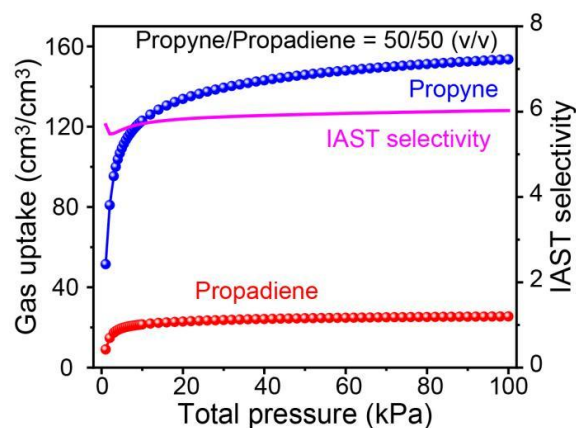
Figure S16. Calculated adsorption isotherms of propyne and propadiene from propyne/propadiene (50/50) mixtures on CuZrF$_6$-TPA at 298 K and IAST selectivity of CuZrF$_6$-TPA towards an equimolar binary mixture.
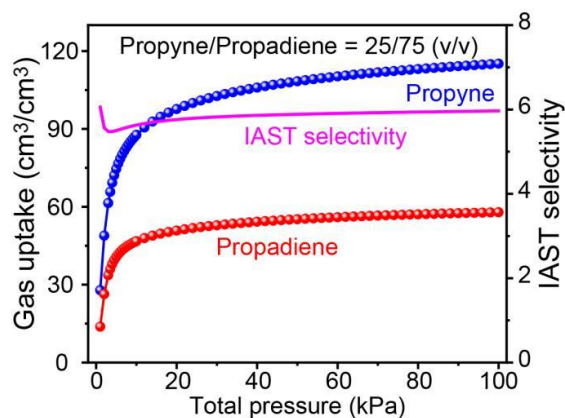
Figure S17. Calculated adsorption isotherms of propyne and propadiene from propyne/propadiene (25/75) mixtures on CuZrF$_6$-TPA at 298 K and IAST selectivity of CuZrF$_6$-TPA towards a 25/75 binary mixture.
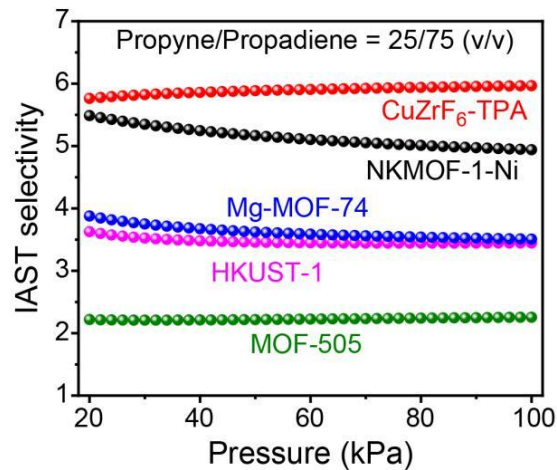
Figure S18. Comparison of IAST selectivity towards a 25/75 mixture of propyne and propadiene of CuZrF$_6$-TPA with other MOFs with OMS.
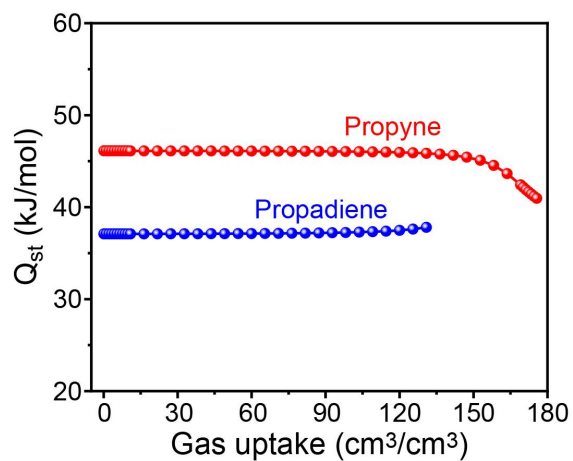
Figure S19. The isosteric heat of adsorption, Qst, for propyne and propadiene in CuZrF$_6$-TPA.
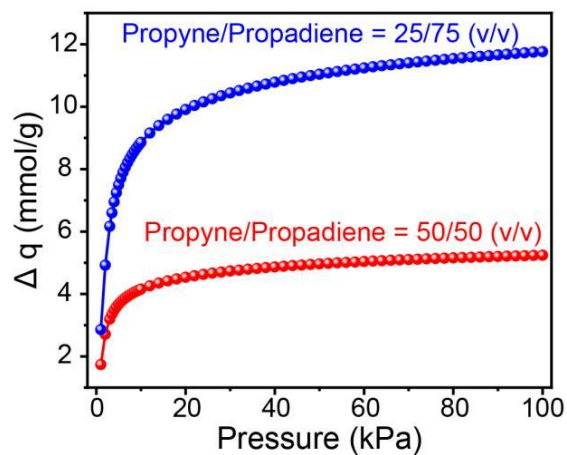
Figure S20. IAST based separation potential for propyne/propadiene (50/50, 25/75) mixtures on $CuZrF_6$-TPA.
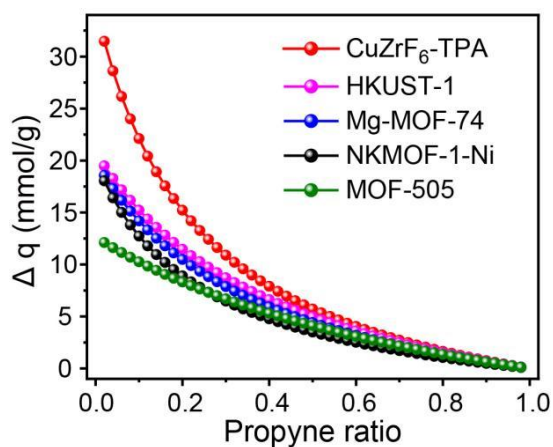
Figure S21. Comparison of the IAST based separation potential for propyne/propadiene mixtures in different proportions on $CuZrF_6$-TPA and reported top performing MOFs.

Table S5. Comparison of the reported materials on properties, propyne adsorption capacity at 50 kPa, IAST selectivity towards propyne/propadiene (50/50), Q_{st}, and IAST based separation potential for propyne/propadiene (50/50).

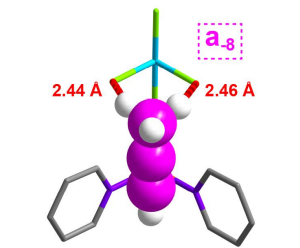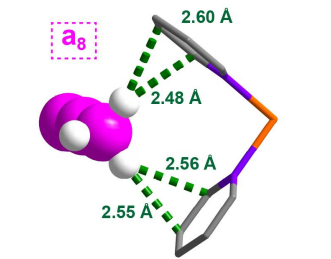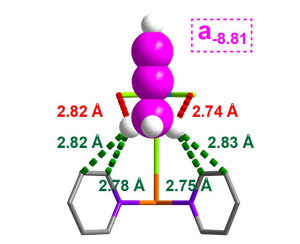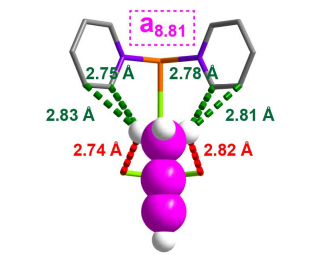| MOFs name	BET surface (m^2/g)	Crystal density (g/cm^3)	Propyne uptake at 50 kPa (cm^3/cm^3)	Propyne uptake at 50 kPa (cm^3/g)	IAST selectivity 50/50	Propyne Q_{st} (kJ/mol)	Δq 50/50 $(mmol/cm^3)$	Δq 50/50 (mmol/g)	Ref
NKMOF-1-Ni	382	1.713	110.13	64.29	4.8	65.1	3.51	2.05	1/2
HKUST-1	1850	0.879	191.97	218.40	3.4	46.3	4.96	5.64	1
MOF-505	1830	0.992	230.87	232.74	2.3	77.4	4.12	4.15	1
Mg-MOF-74	1415	0.920	170.22	185.03	3.5	53.1	4.41	4.79	1
CuZrF$_6$-TPA	**1333**	**1.091**	**177.42**	**162.62**	**6.0**	**46.1**	**5.72**	**5.24**	**This work**

References：
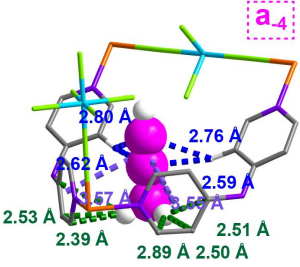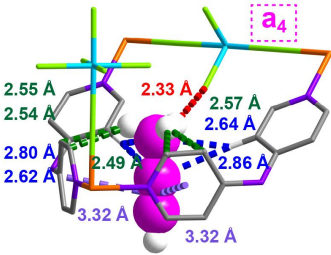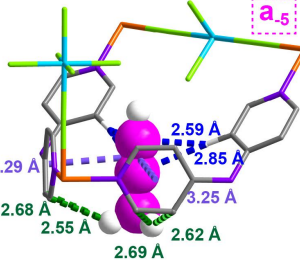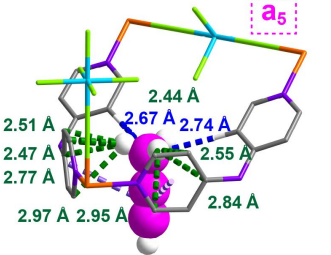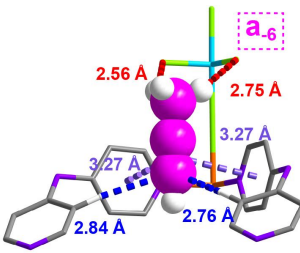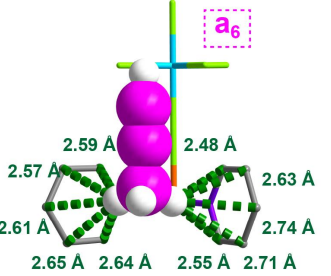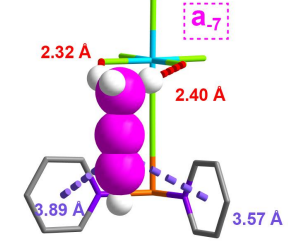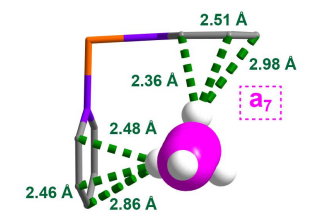
[1] Peng, Y.-L.; Wang, T.; Jin, C.; Deng, C.-H.; Zhao, Y.; Liu, W.; Forrest, K. A.; Krishna, R.; Chen, Y.; Pham, T.; Space, B.; Cheng, P.; Zaworotko, M. J.; Zhang, Z. Efficient propyne/propadiene separation by microporous crystalline physiadsorbents. *Nat. Commun.* **2021**, *12*, 5768.

[2] Peng, Y.-L.; He, C.; Pham, T.; Wang, T.; Li, P.; Krishna, R.; Forrest, K. A.; Hogan, A.; Shanelle, S.; Space, B.; Fang, M.; Chen, Y.; Zaworotko, M. J.; Li, J.; Li, L.; Zhang, Z.; Cheng, P.; Chen, B. Robust Microporous Metal-Organic Frameworks for Highly Efficient and Simultaneous Removal of Propyne and Propadiene from Propylene. *Angew. Chem. Int. Ed.* **2019**, *58*, 10209–10214.

IV DFT calculation

Table S6. Illustration of a propyne molecule crossing the windows in CuZrF6-TPA for calculating the interaction energy.

|	
(a₀)	$\Delta E=$ -64.12 KJ/mol
(a₋₁)	$\Delta E=$ -44.73 KJ/mol
(a₁)	$\Delta E=$ -77.40 KJ/mol
(a₋₂)	$\Delta E=$ -38.14 KJ/mol
(a₂)	$\Delta E=$-83.18 KJ/mol
(a₋₃)	$\Delta E=$ -44.31 KJ/mol
(a₃)	$\Delta E=$ -75.77 KJ/mol

a₋₄	ΔE= -41.31 KJ/mol	a₄	ΔE= -44.54 KJ/mol
a₋₅	ΔE= -52.81 KJ/mol	a₅	ΔE= -34.92 KJ/mol
a₋₆	ΔE= -64.94 KJ/mol	a₆	ΔE= -37.20 KJ/mol
a₋₇	ΔE= -57.45 KJ/mol	a₇	ΔE= -22.05 KJ/mol
a₋₈	ΔE= -54.23 KJ/mol	a₈	ΔE= -30.06 KJ/mol
a_{-8.81}	ΔE= -43.42 KJ/mol	a_{8.81}	ΔE= -42.78 KJ/mol

Table S7. Illustration of a propadiene molecule crossing the windows in CuZrF6-TPA for calculating the interaction energy.

	b₀	ΔE= -57.98 KJ/mol
b₋₁	ΔE= -55.23 KJ/mol	b₁
		ΔE= -51.63 KJ/mol
b₋₂	ΔE= -56.93 KJ/mol	b₂
		ΔE=-61.67 KJ/mol
b₋₃	ΔE= -66.77 KJ/mol	b₃
		ΔE= -64.79 KJ/mol

|	ΔE= -53.66 KJ/mol		ΔE= -55.89 KJ/mol
	ΔE= -55.38 KJ/mol		ΔE= -52.98 KJ/mol
	ΔE= -52.53 KJ/mol		ΔE= -48.69 KJ/mol
	ΔE= -46.53 KJ/mol		ΔE= -44.08 KJ/mol
	ΔE= -42.66 KJ/mol		ΔE= -41.39 KJ/mol
	ΔE= -40.99 KJ/mol		ΔE= -41.53 KJ/mol

V   Breakthrough simulations and experiments
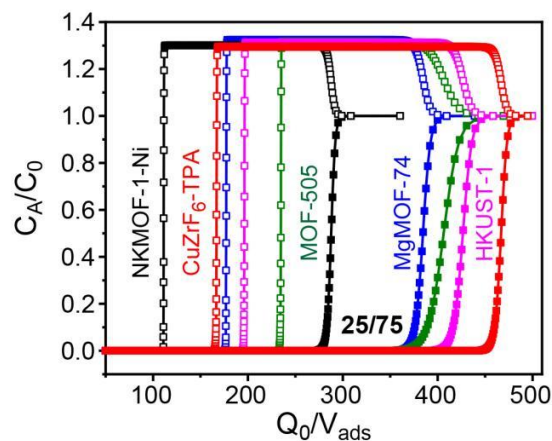
Figure S22. Simulated breakthrough curves of CuZrF$_6$-TPA and other top-performing materials for propyne/propadiene (25/75) mixtures.
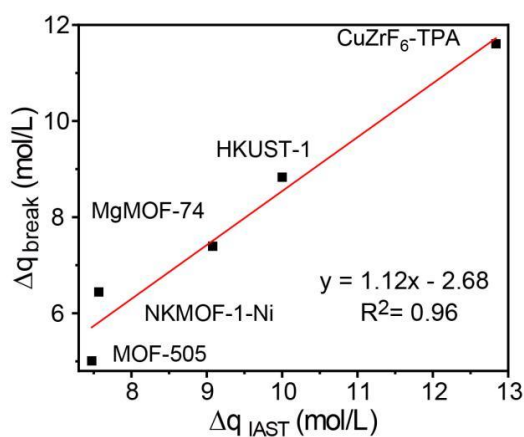

Figure S23. Plots of the calculated productivity of propadiene in > 99.996% purity and separation potential Δq_{IAST} from propyne/propadiene (25/75).
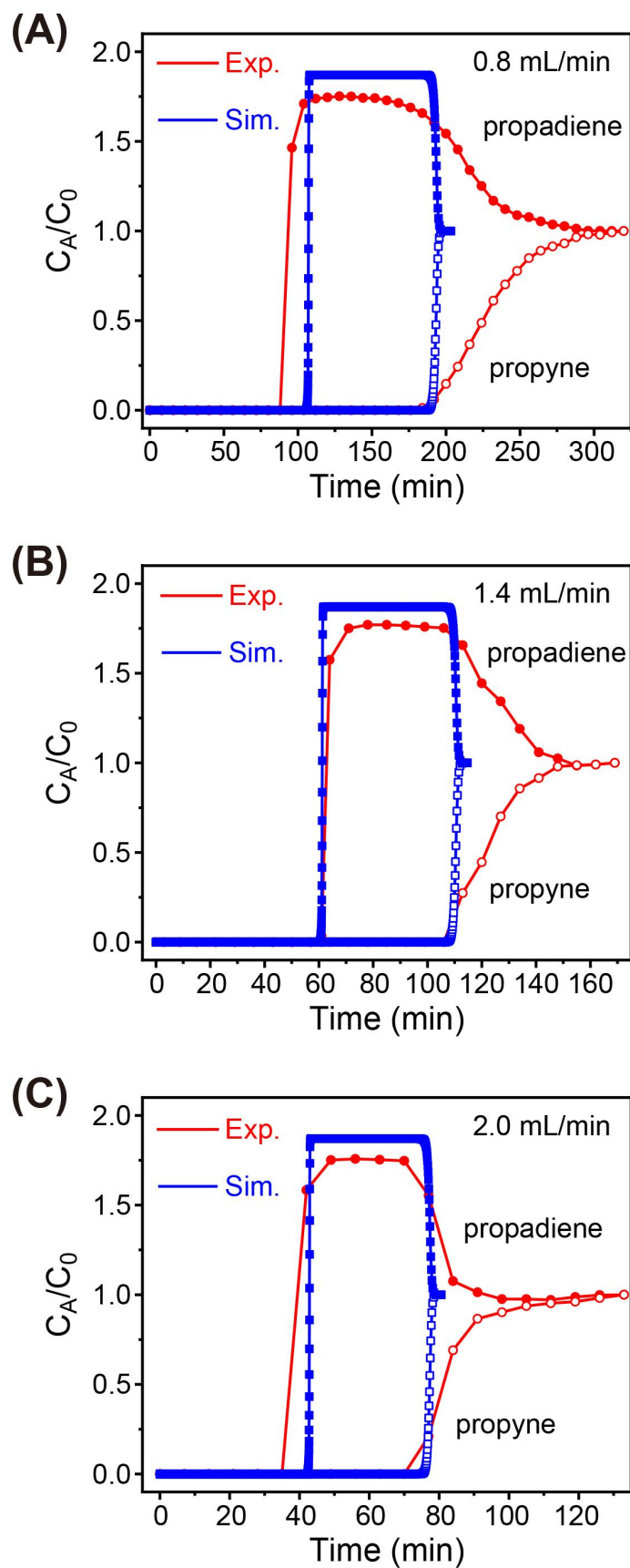
Figure S24. Conparison of the experimental and simulated breakthrough curves of CuZrF$_6$-TPA for propyne/propadiene (50/50) under different flowrates.
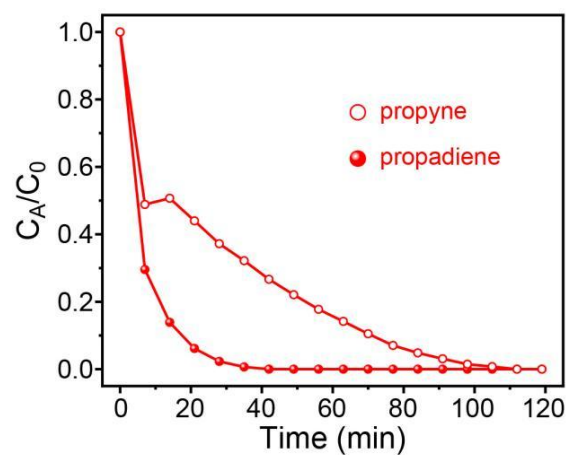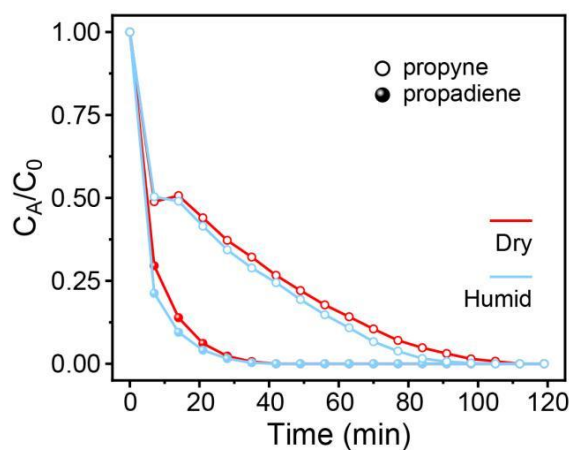
Figure S25. Experimental dynamic desorption curves of CuZrF$_6$-TPA after breakthrough experiment of propyne/propadiene (50/50, 0.8 mL/min). Desorption conditions: Ar flow rate 10 mL/min at 100 °C.
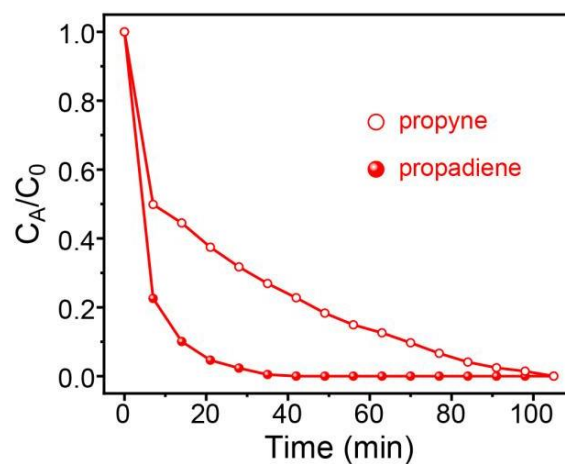
Figure S26. Experimental dynamic desorption curves of CuZrF$_6$-TPA after breakthrough experiment of propyne/propadiene (50/50, 1.4 mL/min). Desorption conditions: Ar flow rate 10 mL/min at 100 °C.
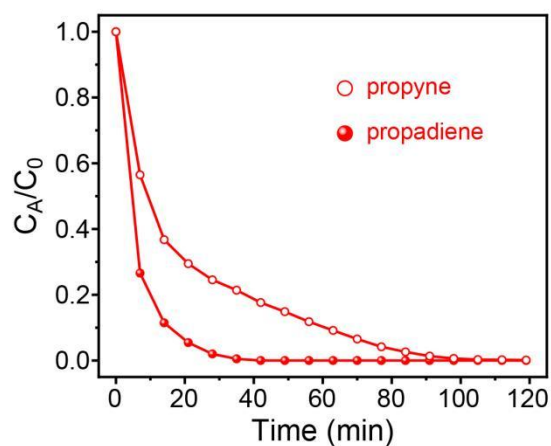
Figure S27. Experimental dynamic desorption curves of CuZrF$_6$-TPA after breakthrough experiment of propyne/propadiene (50/50, 2.0 mL/min). Desorption conditions: Ar flow rate 10 mL/min at 100 °C.

Figure S28. Experimental dynamic desorption curves of CuZrF$_6$-TPA after breakthrough experiments of propyne/propadiene (50/50, 0.8 mL/min) under dry and humid conditions. Desorption conditions: Ar flow rate 10 mL/min at 100 °C.
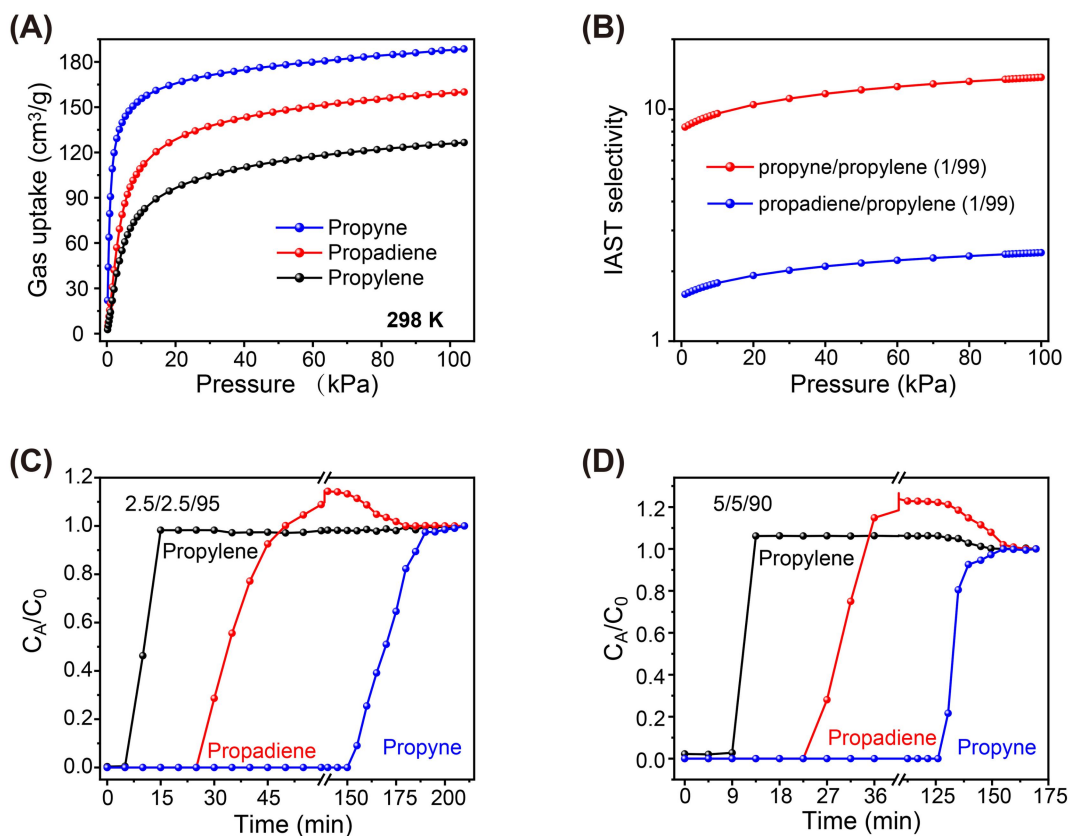
Figure S29. (A) The sorption isotherm of propyne, propadiene and propylene on CuZrF$_6$-TPA at 298 K. (B) IAST selectivity of propyne/propylene and propadiene /propylene. (C, D) Experimental breakthrough curves of CuZrF$_6$-TPA for propyne/propadiene/propylene v/v/v = 2.5/2.5/95 (C) and 5/5/90 (D) at 298 K. Flow rate: 4 mL/min.